Chapter 7
Planetary Ices Attenuation Properties

Christine McCarthy and Julie C. Castillo-Rogez

Abstract In this chapter, we review the topic of energy dissipation in the context of icy satellites experiencing tidal forcing. We describe the physics of mechanical dissipation, also known as attenuation, in polycrystalline ice and discuss the history of laboratory methods used to measure and understand it. Because many factors – such as microstructure, composition and defect state – can influence rheological behavior, we review what is known about the mechanisms responsible for attenuation in ice and what can be inferred from the properties of rocks, metals and ceramics. Since attenuation measured in the laboratory must be carefully scaled to geologic time and to planetary conditions in order to provide realistic extrapolation, we discuss various mechanical models that have been used, with varying degrees of success, to describe attenuation as a function of forcing frequency and temperature. We review the literature in which these models have been used to describe dissipation in the moons of Jupiter and Saturn. Finally, we address gaps in our present knowledge of planetary ice attenuation and provide suggestions for future inquiry.

7.1 Introduction

Planetary satellites are subject to periodic deformation in response to the tides exerted by their primaries. This deformation is driven by the eccentricities of their orbits and by the physical librations of the satellites' shapes. Depending on the internal structure and material properties of these objects, deformation can result in the dissipation of tidal energy in the form of heat, impacting the geophysical

C. McCarthy (✉)
Lamont-Doherty Earth Observatory, Columbia University, Palisades, NY, USA
e-mail: mccarthy@ldeo.columbia.edu

J.C. Castillo-Rogez
Jet Propulsion Laboratory, California Institute of Technology, Pasadena, CA, USA

M.S. Gudipati and J. Castillo-Rogez (eds.), *The Science of Solar System Ices*,
Astrophysics and Space Science Library 356, DOI 10.1007/978-1-4614-3076-6_7,

evolution of the object. Loss of mechanical energy results in tidal evolution of a satellite's orbital and spin properties.

Properly modeling the tidal response of planetary objects is important for two reasons. First, tidal heating can be a significant heat source; it is thought to drive cryovolcanism on Enceladus (Barr and Milkovich 2008) and to be involved in the preservation of a deep ocean in Europa (Tobie et al. 2003), for instance. Second, the tidal response of icy bodies can potentially be measured, in which case the characterization of its amplitude and phase provides direct constraints on the internal and thermal structures of these objects. Methods to measure that tidal response include physical librations of the shape (e.g., Williams et al. 2001), radial deformation of the equatorial bulge (Castillo et al. 2000), secular acceleration (e.g., Aksnes and Franklin 2001), and phase lag (Rappaport et al. 2008). Dynamical models of resonant interactions between satellites may also lead to constraints on their dissipative properties (Zhang and Nimmo 2009). Another aspect of the problem is that the periodic deformation of the shape can promote significant geological activity, for example, by: (1) tectonic stresses leading to crack nucleation and faulting (e.g., terrestrial ice shelves (Rothrock 1975) and cycloid features on Europa (Greenberg et al. 1998)); (2) promotion of motion along faults (e.g., on Earth (Cochran et al. 2004) or on Enceladus, at the Tiger stripes (Hurford et al. 2007)); and (3) volcanic activity (e.g., on Io (Peale et al. 1979)).

In order to infer constraints on the evolution and current state of icy bodies from these various observations, it is necessary to develop models that properly account for the behavior of planetary material subject to tidal stressing in the relevant conditions of frequency, temperature and stress amplitudes. This chapter focuses on the internal friction properties of icy materials – in the viscous and anelastic regimes. Solid-solid friction, another mechanism that can accommodate the response of material to tidal stress, is addressed in the chapter by Erland Schulson.

The response of ice to cyclic deformation has been much studied in conditions relevant to terrestrial ice sheets with geotechnical applications (e.g., Johari et al. 1995) or to model the tidal response of ice shelves and the resulting fatigue-induced cracks (e.g., Cole and Durell 1995). There are very few experiments that have considered the response of ice in conditions relevant to outer planet satellites. Such experiments are technically challenging as they require work in cryogenic conditions, at relatively low stress (below 0.1 MPa) and at frequencies below 10^{-4} Hz (Fig. 7.1). As a result, most tidal models have relied on the extrapolation of data obtained in conditions that may significantly depart from those relevant to icy satellites.

In this chapter, we review the literature available for the mechanical properties of water ice at low frequency approaching conditions in icy satellites, including the mechanisms responsible for dissipation (Sect. 7.2) and examine the variables that can affect the material response in the geologic context (Sect. 7.3). We then look at the models that have been suggested to extrapolate these measurements to conditions relevant to Solar system bodies (Sect. 7.4). Finally, we address the expression of tidal response and its consequences in icy bodies, based on observations and interpretation (Sect. 7.5) and, in light of these considerations, we address a list of related issues and measurements necessary to solve these questions (Sect. 7.6).

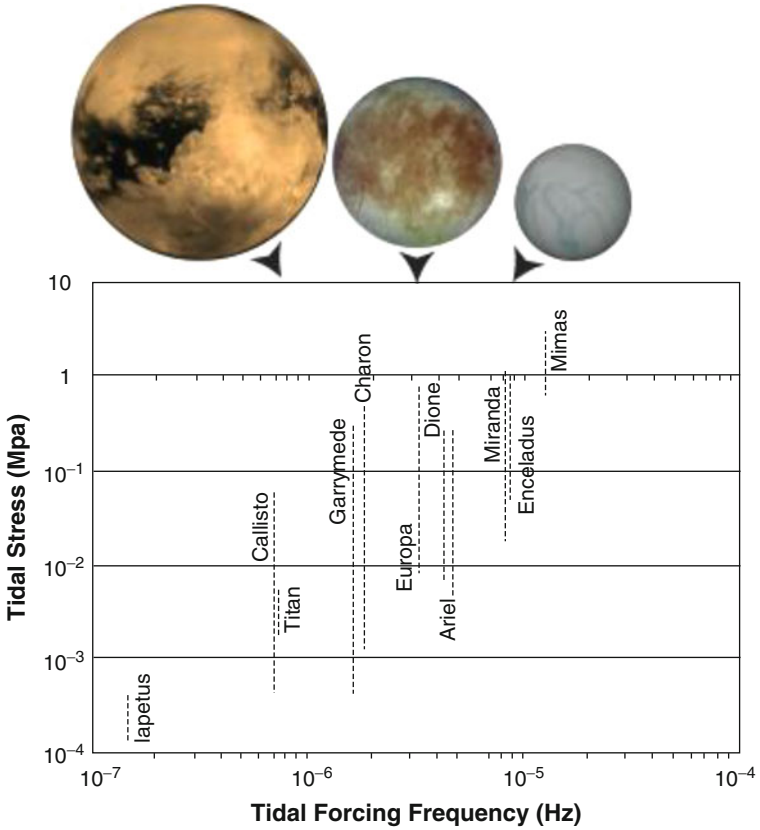

Fig. 7.1 Tidal forcing frequency and cyclic peak stress for the orbital tides at all outer planet satellites. The range of values reflects the possible internal structure models for these objects (*Lower bound* corresponds to models without a deep ocean; *upper bounds* correspond to models with a deep ocean) (Note: satellites figures are not to scale)

7.2 The Physics of Attenuation Under Mechanical Forcing

The study of planetary material anelasticity started in the mid-1950s, mainly focusing on rocky material with the primary goal to support the interpretation of seismic studies (e.g., Faul and Jackson 2005). Our understanding of ice dissipative properties borrows significantly from that research, and we refer the readers to some of the many key papers on the topic: e.g., Jackson (1993), Weertman (1983), Cooper (2002), Karato (2008).

7.2.1 A Few Definitions

Like many materials, ice exhibits viscoelastic behavior. That is, in response to some deviatoric stress, it will respond with a combination of instantaneous elastic

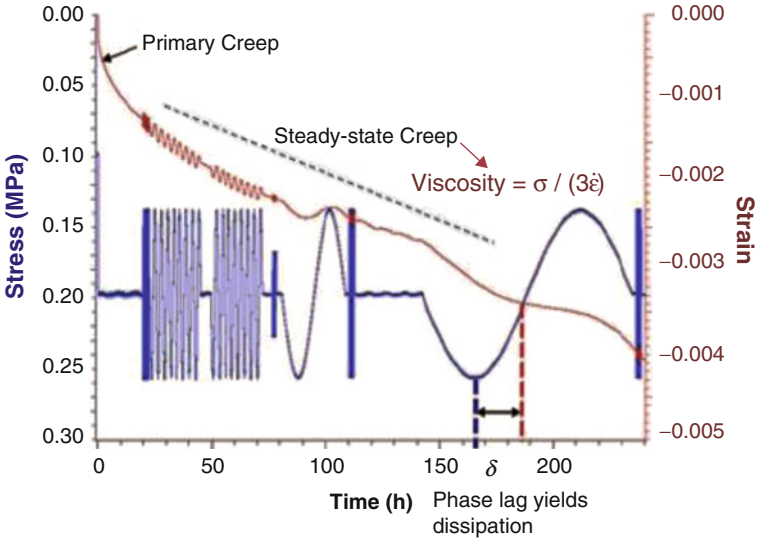

Fig. 7.2 Example of the strain response to a median, or offset, stress in addition to a periodic stress. The response to the offset stress is a typical creep curve with an instantaneous elastic response, a decelerating transient and finally a steady-state response indicated by the monotonic downward trend of the strain data (compression negative). The response to the periodic stress is a periodic strain at the same frequency as the forcing frequency, but lagging behind by δ

behavior and time-dependent inelastic behavior. The characteristic feature of elasticity is that it is completely recoverable; the elastic response merely involves the stretching and contracting of atomic bonds so that, when stress is removed, atoms return to their previous positions. Inelasticity, however, involves time dependent motion of point, line, and planar defects within the crystal. The inelastic response can be broken into two parts: fully recoverable anelastic deformation and permanent viscous (or plastic) creep.[1] These processes are illustrated in Fig. 7.2, which shows the response of a sample of synthetic ice subjected to a constant uniaxial stress, in addition to a periodic stress. The material first exhibits an instantaneous change in length as a consequence of elastic deformation. That first step is followed by a phase of primary creep, during which the strain rate decelerates, until steady-state creep is reached. Primary creep, which is also referred to as "transient creep", may last from a few hours to several tens of hours, depending on the properties of the material and temperature.

It is the inelastic behavior that causes a stressed material to experience a relaxation of elastic strain energy until that energy is fully dissipated. In the case of periodic loading of a viscoelastic material, the dynamic relationship between stress and strain, specifically in terms of the ratio of strain energy dissipated to the energy stored, is described by the term "internal friction", or inverse quality factor Q^{-1}, which is also commonly called attenuation in the earth sciences. Since the various mechanisms responsible for attenuation each have a characteristic time-scale related to the mobility of that defect, the dissipation is very much a function of

the temperature and the frequency of mechanical forcing. A material subject to low temperature and/or rapid forcing has a response that is essentially elastic. On the other hand, a material stressed over a very long period of time at relatively high-temperature has its overall response dominated by its viscosity. Between these two limits is a response that combines a mixture of recoverable and irrecoverable strain, the timescale of which is generally taken as the Maxwell time, that is, the ratio of the material viscosity to its elasticity.

7.2.2 Principles of Laboratory Measurements

Various methods have been used to study viscoelasticity in materials. At high frequencies, resonance methods that measure the decay of free vibrations of a system following a perturbation are typically used. Here, the quality factor is determined from the width of a resonant peak. One resonance method uses ultrasound spectroscopy, in which a specimen is held between two ultrasonic transducers, one acting as a transmitter and the other as a receiver (Lakes 2004). The frequency range of such tests is typically 50 kHz to 20 MHz. It is this technique that has been used extensively to study the internal friction of ice at very low temperature at which point-defect related mechanisms were found to act (Sect. 7.2.4). It is also the only approach used so far that has yielded constraints on the attenuation properties of amorphous ice as a function of its nanoporosity (Sect. 7.3.5).

At conditions applicable to icy satellites (i.e. subresonant, low-frequency conditions of tidal forcing), the desired mode of testing is forced oscillation. Such tests can have either a torsional or longitudinal geometry, and can be either *reversed*, meaning the applied stress (compression-tension) oscillates about zero, or *non-reversed*, in which a median stress is applied in addition to the periodic stress (compression-compression). Longitudinal forced oscillation tests on ice are often conducted with commercial testing machines, where the upper limit in frequency is the instrument resonance and the lower limit is determined by control of drift in electronics and temperature (Lakes 2004). Torsional forced oscillation pendulums have also been used to measure dissipation at subresonant frequencies. In such devices, torque is generated by a motor or an electromagnetic drive and angular displacement of the gripped specimen is measured (i.e., Kê 1947; Woirgard et al. 1977; Vassoille et al. 1978).

In addition to dynamic experiments, the attenuation response of planetary materials has been studied through quasi-static transient microcreep tests. Provided that the rheology is linear, the attenuation spectrum can be determined from the time-dependent creep function using Laplace transform techniques (e.g., Findley et al. 1976; Jackson 1993). As shown in Sect. 7.4.1, microcreep measurements and forced oscillation provide complementary information. Microcreep is an attractive method to probe attenuation properties with a single creep test. However, due to a lack of resolution in microcreep data at short time scales, static methods do not reveal the high frequency dissipation maxima observed in dynamic testing. Additionally, the low frequency transition to purely viscous (permanent) dissipation

predicted by microcreep tests has not been observed, or is possibly not available, from forced oscillation tests. (See Webb and Jackson 2003, e.g., for a comparison between datasets obtained on the same material from these two methods).

7.2.3 Brief History of the Research on Ice Attenuation Properties

The majority of our understanding of ice properties has been obtained from studies on ice shelves and sea ice, focused on geotechnical applications or aimed at understanding the mechanical behavior of ice packs. To the best of our knowledge the first attenuation estimates on ice were obtained in the mid-1950s from analysis of primary creep measurements (Ladanyi and Saint-Pierre 1978; Brill and Camp 1961; Jellinek and Brill 1956). A number of experimental studies also focused on the relaxation of ice at high frequency (e.g., Kuroiwa 1964; Tamura et al. 1986).

The first low-frequency forced oscillation measurements were obtained during the mid-1970s in the Laboratory of Glaciology of Grenoble (e.g., Vassoille et al. 1978; Tatibouet et al. 1981, 1983, 1987). These were torsional measurements obtained over a wide range of temperatures, from 120 to 273 K, and frequencies as low as 10^{-4} Hz. These first experiments probed a regime of attenuation driven by proton reorientation and a grain-boundary absorption mechanism. More recently, the significant bulk of work on dissipation in both laboratory grown and natural sea ice to date has been conducted by David Cole and various coworkers (e.g. Cole 1995, 2001; Cole et al. 1998; Cole and Durell 1995, 2001). A key contribution from Cole (1995) is the development of an empirically-based model to describe relaxation in ice that is specifically tied to microstructure and defect state. This so-called Cole model will be the subject of Sect. 7.4.5.3.

7.2.4 The Physics of Viscoelastic Dissipation in Ice

Energy dissipation within a crystalline material occurs by physical mechanisms that include thermoelasticity, which is relaxation caused by thermal expansion/contraction anisotropy between grains (Zener 1948), and by motion of various types of defects: point-defects within the lattice, linear defects (dislocations), and planar defects (grain, subgrain and phase boundaries). The defect-related mechanisms are the same mechanisms that are responsible for steady-state creep, and as such, are influenced by the same factors: defect density and mobility, temperature, grain size, and stress amplitude, as well as composition and the nature of defects at all scales (including porosity). Evidence that the same defects are involved in the two different responses comes from the determination of activation energies of these processes (e.g., Webb and Jackson 2003). In addition to the mechanisms regularly associated with plasticity and anelasticity in polycrystalline material, ice experiences a large relaxation attributed to its unique and highly disordered structure. The following mechanisms have been associated with viscoelastic dissipation in ice.

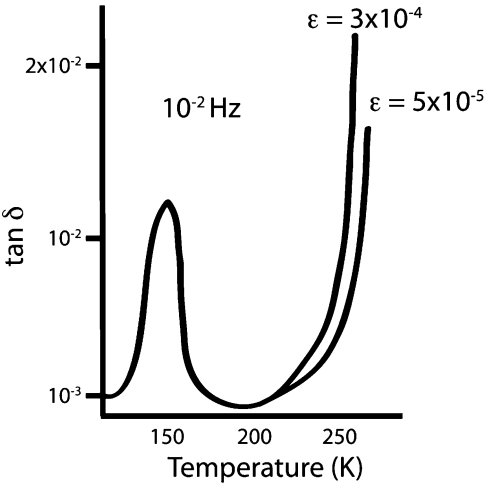

Fig. 7.3 Attenuation versus temperature of single crystal ice displaying a Debye peak at ~150 K associated with proton rearrangement and high-temperature absorption that is strain amplitude dependent at T > 200 K (After Tatibouet et al. 1981)

7.2.4.1 Proton Reorientation

The structure of ordinary Ih ice is such that each H_2O molecule is linked to others by hydrogen bonds in any of six different configurations, meaning that no long-range order in the orientation of H_2O molecules exists (Pauling 1935). Statistically, there are a large number of configurations that the ice structure can take with respect to the orientation of the molecules. A change from one configuration to another comes about either by rotation of molecules or by movement of protons from one oxygen atom to another (Bjerrum 1952). Studies on single crystal ice have revealed a low-temperature (or high frequency) relaxation peak associated with this rearrangement of water molecules by rotational defects (e.g. Vassoille et al. 1978; Hiki and Tamura 1983; Tatibouet et al. 1981). The relaxation is analogous to a Zener relaxation (Zener 1947) in that it occurs because of a change in local atomic order that is affected by the presence of defects (Snoek 1939; Nowick and Berry 1972; p. 349). It takes the form of a Debye peak (seen in Fig. 7.3 centered at ~150 K for $f = 10^{-2}$ Hz), such that there is exponential energy decay associated with (1) a fixed length scale and (2) some loss of bond-energy wrought by application of a deviatoric stress. The presence of dopants has been found to very much affect the motion of protonic point defects, resulting in a shifting of the dissipation peak to lower temperature (Perez et al. 1986) and the creation of a second dissipation peak whose origin remains to be explained (Oguro 2001). The occurrence of proton-reorientation relaxation is expected in cold planetary material (T < 150 K) subject to tidal stress at frequencies between 10^{-5} and 10^{-4} Hz (Castillo-Rogez et al. 2011).

7.2.4.2 Dislocation-Driven Attenuation

An additional influential feature of the Ih ice crystal structure is that the molecules are concentrated close to a series of parallel planes known as the *basal planes*. With the development of the X-ray topographic method in the 1970s, dislocations located on various planes within single ice crystals were observed (e.g., Webb and Hayes 1967; Fukuda et al. 1987; Duval et al. 1983; Baker 1997). The most significant finding from these studies was the remarkable anisotropy in the plastic deformation of ice, such that the creep rate by slip on the basal plane (in particular, the so-called *glide* set of basal planes; Whitworth 1980) is roughly 10^4 times faster, at a given stress, than creep by non-basal slip. Dislocation mobility, which is very low in ice compared to other materials, is related to the level of the Peierls barrier, which is believed to be due in part to the proton disorder described above (e.g., Louchet 2004; Song 2008; Schulson and Duval 2009).

On basal planes, where the Peierls stress is high, attenuation occurs by motion of dislocations (and dissociated partials) via nucleation and migration of geometrical kinks over a Peierls potential hill (e.g., Karato and Spetzler 1990; Karato 1998; Jackson 2007). The simple schematic in Fig. 7.4a demonstrates this type of attenuation mechanism, though, in reality, dislocation loops in the basal plane expand under stress into screw and 60° orientations to take up a hexagonal form, as seen at A in Fig. 7.4b (Ahmad and Whitworth 1988). The purely anelastic relaxation due to the nucleation and migration of a pair of kinks should result in a *Bordoni peak* that is independent of strain amplitude and broader than a peak with a single relaxation time (e.g., Niblett and Zein 1980). The height and shape of the peak are expected to be sensitive to the degree of strain, with a sharper, more defined peak occurring with increased deformation (Nowick and Berry 1972, p. 378). In experiments on polycrystalline ice, Cole and his colleagues applied a uniaxial load that cycled between compression and tension. The zero-mean-stress of their method implied that no plastic deformation occurred during testing, such that no new dislocations were created. They determined, therefore, that observed loss, which showed a shallow frequency dependence and slight drop at the lowest frequency, was due almost entirely to motion of existing dislocations on basal planes, the density of which they controlled by applying various amounts of pre-strain to samples (Cole and Durell 2001).

In more realistic geologic settings, however, relaxation will also be sensitive to the long-term stress. At very low frequency (or high temperature) pinning mechanisms become ineffective and there will be a gradual transition from anelastic to viscous behavior (Karato and Spetzler 1990; Jackson 2007). The transition occurs when single kink nucleations lead to successive nucleation and/or unpinning of dislocations (Karato 1998).

Although the bulk of deformation in polycrystalline ice occurs by slip on basal glide planes, not every grain can be kinematically oriented favorably. On non-basal planes, where the Peierls stress is low, dislocations are instead curved, as seen at S in Fig. 7.4d (Ahmad and Whitworth 1988). Although edge dislocations can move

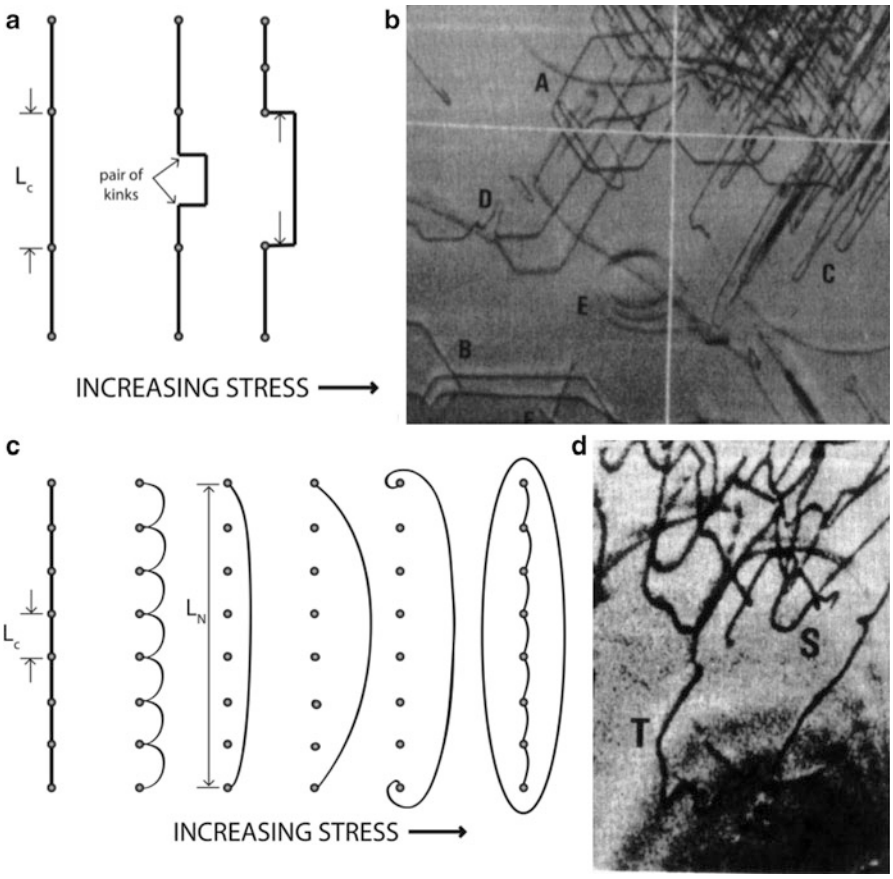

Fig. 7.4 Schematics of dislocation-based dissipation mechanisms and examples of such dislocations in X-ray topography images of single crystals of ice: (**a**) the formation and migration of kink pairs on basal planes where Peierls stress is high, as described by Karato (2008); (**b**) straight and hexagonal loop (A) dislocation segments on the basal plane (Ahmad and Whitworth 1988); (**c**) the bowing out and eventual breakaway of a dislocation segment in a glide plane with low Peierls stress, as described by the Granato-Lücke model (1945), and (**d**) curved dislocation segments in non-basal (possibly pyramidal) planes (Ahmad and Whitworth 1988) with permission from Taylor & Francis Ltd. http://www.tandfonline.com

very fast on non-basal planes, screw dislocations cannot glide at all. Therefore, macroscopic slip on non-basal planes is extremely difficult. However, small-scale anelastic relaxation from oscillating dislocations on these planes is likely an additional contribution to attenuation. The prevailing model for this type of low Peierls stress, dislocation-based damping is that proposed by Granato and Lücke (1956), which describes a three-dimensional network of pinned dislocations behaving like stretched vibrating strings that are pinned at the ends (a distance L_N apart), perhaps by other quasi-immobile dislocations (Tatibouet et al. 1986). They are also pinned at various points along their lengths, the average distance between which is L_C (Fig. 7.4c).

The pinned dislocations oscillate between one equilibrium position and another under alternating stress. With increasing stress amplitude, motion of the dislocation segments transitions from bowing out between pinners to partial breakaway to eventual catastrophic breakaway (Burdett and Queen 1970). Although the Granato-Lücke model has not been well constrained in ice, some form of dislocation breakaway and multiplication is needed to explain the high-temperature, strain-amplitude-dependent attenuation that is observed in ice (Fig. 7.3).

7.2.4.3 Grain-Boundary Sliding (GBS)

Grain boundaries are planar defects in polycrystalline materials that have long been identified as important players in both plastic deformation and energy dissipation. In reality, grain boundaries are far from planar and instead are curved or jagged interfaces. Sliding on nonplanar surfaces can only occur for very small distances before configurational incompatibilities cause stress concentrations at triple junctions to develop (Kê 1946; Raj and Ashby 1971; Raj 1975). Further sliding requires accommodation by one or more of the following: localized elastic deformation of grains (described below); grain-scale diffusive flux of atoms (Ashby and Verrall 1973) or by motion of lattice dislocations (e.g., Kê 1999). For the diffusional mechanism, a rapid flux of matter away from high-traction triple junctions occurs in response to the steep stress gradient along grain boundaries. When diffusive flux is responsible for dissipation, the attenuation spectra takes on a weak frequency dependence that persists for many decades of frequency. Often called the "high-temperature background," this power law absorption (i.e. $Q^{-1} \propto f^{-m}$ where m is between 1/2 and 1/3) has been observed for many materials at high homologous temperature and has been attributed to the diffusion-effected evolution of normal traction on grain, subgrain and/or phase boundaries (Gribb and Cooper 1998; McMillan et al. 2003; McCarthy et al. 2011b).

Recent experimental studies on polycrystalline ice in which samples experienced both a periodic and a long-term constant stress observed moderate power law relationship similar in form to that of silicates (e.g., McCarthy et al. 2008). Because the diffusivity of ice at its melting point is three to four orders of magnitude less than values found for silicate minerals and metals, diffusion-driven relaxation of stress is slow, and the mechanism only becomes dominant when the stress and material geometry become less favorable for other deformation mechanisms. Although diffusion-based creep mechanisms have not been directly observed in water ice at laboratory conditions, such mechanisms are predicted by theory to be expressed under very low stress and in very fine-grained samples (e.g., Goldsby and Kohlstedt 2001). That the dynamic response of polycrystalline ice simultaneously deforming with non-Newtonian rheology revealed a high-temperature background of the same form found in silicate minerals (with Newtonian rheology) is therefore remarkable. It suggests that, despite creeping by non-Newtonian deformation mechanisms of dislocation-accomodated grain boundary sliding and dislocation creep, the small periodic stress potential of forced oscillation experiments samples

an additional mechanism, that of chemical diffusion at grain (or subgrain) boundaries, or by some mechanism that supplies a distribution of compliances to give the characteristic broad band of attenuation. This needs to be moderated however by the presence of impurities and partial melt, which are expected to modify the material geometry and effect the expression of grain boundary sliding (see further details in Sect. 7.5).

An additional dissipation mechanism attributed to grain boundaries has been observed in the form of a plateau in the high frequency range of attenuation spectra in some materials. The shape of the spectra has commonly been attributed to the superposition of a Debye peak associated with "elastically-accommodated grain boundary sliding" (e.g., Kê 1947). According to classical theory, grain boundary sliding at high frequency and/or low temperature is accommodated not by diffusion but instead by local elastic deformation of grains (Raj and Ashby 1971). In that sense, this mechanism may be the geometrically needed first step to long-range diffusionally accommodated grain boundary sliding discussed above (Barnhoorn et al. 2007; Sundberg and Cooper 2010). The mechanism is considered to be rate-limited by grain boundary viscosity.

Dynamic studies on non-deformed and annealed samples of polycrystalline ice have confirmed the presence of an attenuation peak at high temperatures attributed to grain boundary sliding (Cole et al. 1998). Interestingly, samples that were strained to 1% showed an increase in the high-temperature background attenuation that caused the grain boundary peak to nearly disappear (Tatibouet et al. 1987). These works suggest that the anelastic response of polycrystalline ice at high temperature is due to a combined effect of dislocation and grain boundary sliding-based mechanisms, such that strain history is critical to the response.

7.2.5 *Shear Versus Bulk Viscoelasticity*

Outer planet satellites are subject to both compression-extension and shear stresses that result from the combination of a radial component and a librational component (phase lag of the equatorial bulge) (Murray and Dermott 2000; Greenberg et al. 1998, their Figure 1). The radial component is a function of the material attenuation properties under compression while the librational component produces shear deformation of the material, and the associated dissipated energy is thus a function of the shear dissipation factor.

Most forced oscillation experiments on polycrystalline ice have used uniaxial loading and, thus, measured the Young's modulus E dissipation, Q_E^{-1}, which is a combination of bulk k and shear μ moduli dissipation according to:

$$Q_E^{-1} = \frac{\mu}{3k+\mu} Q_k^{-1} + \frac{3k}{3k+\mu} Q_\mu^{-1}. \tag{7.1}$$

Using the standard relationships between elastic moduli and the Poisson's ratio of ice (0.325) means that Young's modulus type experiments on polycrystalline ice measure $Q_E^{-1} \cong 0.12\,Q_k^{-1} + 0.88\,Q_\mu^{-1}$. Therefore, care must be taken to use the appropriate loading mode of dissipation when applying laboratory data to tidal stress modeling and when comparing ice attenuation measurements to those of rocky materials, which are traditionally obtained in a torsional geometry (i.e., $100\%Q_\mu^{-1}$).

Another consideration is related to the significant anisotropy of monocrystalline ice (Young's modulus of ~8 GPa along the *a*-axis vs. 11.5 GPa along the *c*-axis) and how this is expected to influence anelastic properties. Although an aggregate with randomly dispersed grains can be treated as an isotropic solid behaving independently from orientation, ice that has aligned grains, i.e. a fabric, cannot be treated so simply. Strain-induced anisotropy in polar ice, for instance, is known to significantly affect shear viscosity (e.g., Staroszczyk and Morland 1999). Studies on unidirectionally solidified first-year sea ice found that anisotropy affects attenuation as well. Specifically, the magnitude of dissipation was found to be proportional to an orientation factor, which is determined by the average shear stress resolved on basal planes (Cole et al. 1998). So application of attenuation measurements made on laboratory prepared isotropic ice to actively deforming icy shells (where fabric formation is certainly possible) is not straightforward.

7.2.6 Linear and Non-linear Deformation

At high enough levels of strain, all materials will display some nonlinear effect or strain amplitude-dependence. Single crystals of ice tested at laboratory conditions have shown a distinct nonlinearity at strains as low as 2×10^{-5} (Fig. 7.3). The higher the temperature and lower the frequency, the more pronounced the strain-amplitude dependence (Tatibouet et al. 1986). Amplitude-dependent attenuation has been observed in polycrystalline ice as well (Cole and Durell 1995; Tatibouet et al. 1981). For the temperatures and frequencies tested by Cole and Durell (1995), decreasing anelasticity with decreasing peak stress that was quasi-linear for stresses smaller than 0.3 MPa was observed and tended toward zero as stress decreased.

Strains as high as 2×10^{-5} are expected in the icy shells of outer planet satellites such as Europa (Tobie et al. 2003) and Enceladus (Nimmo et al. 2007). Therefore it is reasonable to expect some nonlinearity in the response of the shell material. In that case, some basic assumptions about viscoelasticity break down. For instance, the transition to fully viscous behavior does not necessarily correspond to the Maxwell time. Thus, it is possible that, even if the tidal forcing frequency is close to the material's Maxwell frequency, a Maxwell solid model (Sect. 7.4.4.1) may underestimate the amount of dissipation resulting from cyclic stressing.

7.3 Laboratory Measurements on Planetary Ices: State of the Art

In the previous section we addressed the state of knowledge of attenuation in crystalline water ice. However, planetary ices encompass a wide range of composition in the form of second-phase impurities. Of specific relevance is the presence of a variety of hydrates: ammonia and methanol hydrates, hydrated salts, clathrate hydrates (see chapters by de Bergh et al. and Choukroun et al. in this book). The influence of these species on the overall behavior of a mixture of icy material depends on the form under which they condensed in the ice: soluble species at the grain boundaries, dopants within the ice lattice, or condensates within the ice matrix. Another important problem addressed in this section is the role of microstructure on attenuation and its evolution as a consequence of accumulated strain. We also briefly address the state of knowledge about dissipation properties of amorphous ice, because of its relevance to binary Kuiper Belt Objects.

7.3.1 Dopants and Soluble Impurities

Impurities in ice may be present within the crystal lattice as dopants or localized at grain boundaries. Dopants of relevance to icy satellites are ammonia and various chlorides. These particles can enter the lattice and increase the dissipation at a given temperature. The impact of various impurities on the attenuation associated with proton reorientation has been studied. Dopants (both KOH and HF) tend to decrease the temperature at which the proton-ordering associated maximum of dissipation is encountered at a given frequency (Perez et al. 1986; Oguro 2001; see also a review by Petrenko and Whitworth 1999). Studies have also focused on the influence of doping on dislocation-based damping in single crystal and polycrystalline ice. The bonding environment in the presence of HF molecules is such that dislocations can move more rapidly, thus weakening the ice and resulting in higher attenuation and larger strain-amplitude dependence (Perez et al. 1986; Tatibouet et al. 1986). Additionally, HF-doping of polycrystalline ice causes a peak associated with grain boundaries to move to higher temperature (Tatibouet et al. 1987).

7.3.2 Partial Melting and Slurries

The role of partial melt in the dissipation of planetary materials has been investigated experimentally for a variety of silicates and oxides in an effort to link seismic observation with a partially molten, low seismic velocity zone in the earth. In the case of terrestrial rocks, various studies have shown that a few percent of melt is sufficient to significantly increase dissipation (e.g., James et al. 2004;

Fountaine et al. 2005). The mechanisms by which melt influences wave velocity, modulus and attenuation are known as the "poroelastic effect" and the "anelastic effect". Poroelastic effects are due to the large compressibility and little to no rigidity in the melt phase resulting in a decrease in elastic moduli of the solid-liquid composite. Energy dissipation occurs via "squirt flow" of viscous melt between neighboring pores (Mavko 1980). Extensive theoretical studies have been performed on this poroelastic effect to determine the modulus reduction and timescale of relaxation based on the geometry of the system and the melt fraction and viscosity (e.g., O'Connell and Budiansky 1977; Mavko et al. 1998). Unless the pore aspect ratio is very small, the characteristic frequency for the poroelastic effect on Q^{-1} is much higher than the seismic frequency range.

The anelastic effect of partial melt is the enhancement of grain boundary sliding. The specific anelastic response of partially molten systems is believed to be strongly influenced by melt geometry (e.g., Mavko 1980), that is, by the wetting behavior of the melt with respect to the crystalline solid, which is determined by the interfacial energies of the solid/melt system (e.g., Nye and Frank 1973; Waff and Bulau 1979). In the case of silicate partial melt systems, the general consensus is that melt resides in an interconnected network of triple grain junctions. Several studies found that the presence of a texturally equilibrated melt phase does little to the steady-state Newtonian (Cooper and Kohlstedt 1984) and non-Newtonian (power law) (Beeman and Kohlstedt 1993) creep behavior, other than create a minor enhancement of creep rate due to the reduction in diffusive path length. The increase in attenuation in specimens with such melt geometry was solely attributed to the viscosity decrease; the melt-bearing samples presented the same attenuation "band" observed in melt-free samples (Gribb and Cooper 2000).

(1) When interfacial energies instead dictate a completely wetted grain boundary, (2) where lenses and larger pockets of melt are present (Faul et al. 2004), or (3) in the case of non-equilibrium geometries (Fountaine et al. 2005), a broad dissipation peak superimposed on the background has additionally been observed and attributed to enhancement of elastically-accommodated grain boundary sliding (see Sect. 7.2.4) (Faul et al. 2004; Jackson et al. 2006). The relaxation timescale is dependent on melt viscosity and the aspect ratio of grain boundary regions such that the position and dimensions of the absorption peak evolve as the fraction of melt increases. Dissipation has been found to increase as the melt fraction increases up to 25% (Fountaine et al. 2005).

The dihedral angle of ice and water is approximately 20° and thus the equilibrium form should consist of channels of water at three-grain intersections (Nye and Frank 1973). However, significant variation in equilibrium geometry (e.g., Mader 1992) and thin films at grain boundaries (Dash et al. 2006) have also been observed in polycrystalline ice, even at subsolidus temperatures. Small amounts of impurities, which are driven from grains during crystallization and therefore concentrate at grain boundaries, are known to greatly enhance complete surface melting. Though a thorough examination of attenuation in ice + melt systems has not yet been conducted, Cole and Durell (1995) observed a decrease in modulus and increase in anelasticity above the eutectic melting temperature in laboratory-grown saline samples.

Both the elastic and anelastic responses were amplified with increased salt content, consistent with previous observations made via resonance techniques (Spetzler and Anderson 1968). The effect of partial melt on ice properties is particularly significant in planetary settings where the auxiliary phase results in a deep eutectic with ice, such as with sulfuric acid or ammonia. The icy shells of satellites with such chemistry could consist of a significant melt phase. Thus the effect of partial melt on the attenuation of ice is a topic of continued interest.

7.3.3 Solid Particles and Second Phases

Solid particles, such as silicates, and second phases, such as hydrates, located at the grain boundary region may play a significant role in grain boundary sliding. Theoretical studies determined that unless solid particles are of the order of a few nanometers, they most likely inhibit diffusion at the grain boundaries (Raj and Ashby 1971). Experimentally, it has been found that second phases impede grain boundary sliding, increase viscosity, and thus limit internal friction at low stress (e.g., Jackson et al. 2002 for silicates; Song et al. 2006 for ice). Although inhibition of GBS is expected to decrease attenuation in a two-phase system at low stress, this is countered by the increase of dislocation density and an additional mechanism of dissipation at heterophase boundaries (Buechner et al. 1999). However, above a certain stress, pile-ups of dislocations at phase boundaries cause local stress concentrations that result in multiplication of dislocations and/or fracture of second phases, thus enhancing the creep rate (McCarthy et al. 2011a). The idea that softening can occur at high stress raises an important question as to the applicability to icy satellites. It implies that the impact of silicates and other second phases on the rheology of icy satellite material is a function of tidal stress amplitudes. In general, the increase of viscosity due to silicates is inferred from empirical relationships established by measurements obtained at relatively large stress (e.g., Friedson and Stevenson 1983) in comparison to the tidal stress amplitude of icy satellites. These authors considered a low content of silicate grains (<4 vol%). For a high content of silicates, jamming between silicate grains may become the main feature limiting creep, as demonstrated by the experimental work of Durham et al. (2009). Silicate particles also act in preventing grain growth, which indirectly influences the mechanical properties of the material (Goodman et al. 1977; Barr and Milkovich 2008).

7.3.4 Porosity

Several theoretical studies have been developed to estimate the decrease in elastic moduli due to porosity and/or cracks based on the geometry and volume fraction of cavities (e.g., Kuster and Toksöz 1974; Wu 1966; Mavko et al. 1998). The analysis is identical to the case of fluid-filled pores but, here, the modulus of the dry or empty

inclusion is zero. For both saline and non-saline low porosity ice ($\phi < 0.1$), a decrease in effective Young's modulus has been observed (Cole 1995; Cole and Durell 1995) and found to follow the form: $E(GPa) = 10.0–35.1\phi$ (Langleben and Pounder 1963). It has been posited that in small icy satellites (<1000 km in radius), modest self-gravitation further decreases effective modulus, which should enhance the tidal evolution of binary asteroids (Goldreich and Sari 2009).

Studies have also investigated the influence of porosity on energy dissipation. One source of relaxation for cracked or porous solids is related to relaxation of shear stress within each pore. The characteristic relaxation frequency for the mechanisms is $\omega \approx (\mu/\eta)(c/a)$ where μ is the shear modulus of the solid, η of the fluid (or zero viscosity void) and c/a is the aspect ratio of the void, so that, unless the aspect ratio of voids is extremely small, the characteristic frequency is in the MHz range (O'Connell and Budiansky 1977). That an increase in attenuation with increased porosity was observed at low frequencies in saline ice (Cole and Durell 1995) suggests that the relaxation was due, not to gas filled pores, but to fluid moving through very small aspect ratio cracks or brine channels. Since the measurements were made on saline ice at temperatures well above the eutectic melting temperature, this can reasonably assumed to be the case. Increased attenuation in 1% saline ice in the kHz range has been interpreted as flow between fluid pockets with aspect ratio 10^{-3} (Spetzler and Anderson 1968; O'Connell and Budiansky 1977).

Other studies on porosity consider the case of a granular (i.e., unsintered) material typical of rubble-piles (e.g., Pilbeam and Vaisnys 1973). For these cohesionless soils, energy dissipation is caused by friction at grain-to-grain contacts and is sensitive to confining pressure. If the shear stress amplitude is less than the product of the normal force and the coefficient of friction, then the main source of mechanical loss is by static friction at the grain boundaries (e.g., Mindlin 1954; Pilbeam and Vaisnys 1973; Winkler and Murphy 1995). Experimental data gathered in the final reference indicates that the effective dissipation factor corresponding to static friction is on the order of 100–1000 under pressure conditions ($P < 10$ MPa) relevant to small irregular satellites, like Janus and Epimetheus. Porosity in such settings would greatly influence the acoustic properties of the icy shell and possibly the attenuation at seismic frequencies, depending on the shape of cavities. Acoustic methods have been very successful in measuring porosity in geologic and engineering materials. However, at frequencies relevant to tidal forcing of icy satellites, there is no reason to expect anelastic dissipation due to porosity.

However, when shear stress exceeds the confining pressure, macroscopic frictional sliding between grains results in dissipation that is strain amplitude dependent and that decreases with confining pressure. Details about the physics driving frictional sliding can be found in the chapter by Erland Schulson. That problem has been approached by Nimmo et al. (2007) in the case of friction along Enceladus' Tiger stripes.

7.3.5 Amorphous Ice

Constraints on the mechanical properties of amorphous ice are scarce. To the best of our knowledge, no data has been obtained on the attenuation properties of amorphous ice under conditions relevant to planetary bodies. As amorphous ice is difficult to produce in laboratory and is mostly handled in the form of thin films formed under a low-vapor atmosphere on a cold plate at temperatures below 100 K, the only method so far to test their attenuation properties is with a vibrating plate in the kHz-MHz frequency range (see Sect. 7.2.2). Such experiments carried out by Hessinger et al. (1996) proved a very useful approach for constraining the amount of nanoporosity in low-density amorphous ice. At these frequencies, the quality factor is very sensitive to nanoporosity so that a freshly deposited amorphous ice sample is characterized by a small value of Q (on the order of 10). That parameter increased as the sample was warmed up and the porosity annealed, as indicated by an increase of the ice density.

Attenuation data are also lacking for other rare forms of ice that are believed to be present in planetary bodies but are difficult to produce in the lab, such as cubic ice and high-density forms of amorphous ice.

7.3.6 Material Aging

In polycrystalline material, various mechanisms are expected to play a role in the aging of the samples: grain growth, recrystallization, and rearrangement of dislocations (e.g., Taupin et al. 2008). The effect of aging is a common phenomenon largely studied in materials science. Tatibouet et al. (1981) studied the effects of both thermal aging and plastic aging and found that thermal aging of monocrystalline ice is characterized by an increase in internal friction (under torsion) and that plastic aging enhances the total aging rate. Plastic aging results from the multiplication of dislocations as a consequence of Frank-Read source mechanisms (e.g., Tatibouet et al. 1981) and their accumulation as an effect of viscous strain. The stress at which these dislocations form decreases with increasing temperature (e.g., Goldsby 2007).

Tatibouet et al. (1981) also show that accumulation of dislocations during aging can lead to polyganization of the ice. Johari et al. (1995) measured the complex Young's modulus of aged polycrystalline ice samples and observed a decrease in effective modulus by 30% after only ~30 h of sample aging, after which that modulus reached equilibrium. For their coarse-grain samples and temperatures in the 240–260 K range, phase lag continuously increased for the first ~50 h of testing; this parameter then decreased and seemed to reach an equilibrium (or at least evolve slowly) by the end of the 240-h long test. Thus, while the change in elastic properties rapidly reached equilibrium, the internal friction in these samples evolved on a longer timescale. However, after several hundred hours of aging (thermal or plastic), these authors observed a decrease in internal friction, which they interpreted as a result of a change in dislocation density. Cole and Durell (2001) interpreted the decrease in internal friction as dynamic recovery under low stress.

7.4 Quantifying Viscoelasticity and Attenuation

Deformation in a geologic setting involves mechanisms acting over a range of time scales. Some mechanisms can be easily captured by steady-state creep experiments. Others, which represent only small deviations from purely elastic behavior, involve strains so small as to be nearly undetectable by creep experiments. Instead, attenuation experiments "tickle" a material by applying a very small dynamic load. Here we supply the mathematical relationships between the static (creep) response and dynamic response and provide a summary of various mechanical models that have been used to describe the viscoelasticity of ice and other planetary materials.

7.4.1 Stress–Strain Relationships in the Time Domain

The steady-state creep response of water ice has been studied a great deal, and several decades of laboratory measurements have led to the identification of empirical relationships that can predict the viscosity of water ice for a wide range of conditions. It is beyond the scope of this chapter to address the origin and development of these relationships, and we refer readers to key references and detailed reviews on the topic: Goodman et al. (1981), Duval et al. (1983), Weertman (1983), Goldsby and Kohlstedt (2001), Durham and Stern (2001), Castelnau et al. (2008).

The relationship between strain rate and differential stress, temperature, and grain size is generally quantified by the semi-empirical power law:

$$\dot{\varepsilon} = A\frac{\sigma^n}{d^p}\exp\left(\frac{-E_a^*}{RT}\right), \tag{7.2}$$

where A is a factor associated with aspects of microstructure (exclusive of grain size), chemical potentials and geometry, n and p are constants that reflect the (power law) sensitivities to σ the stress, d the grain size, E_a corresponds to the activation energy, R is the gas constant, and T the temperature. Although all thermally activated mechanisms will be operating simultaneously in a stressed system, at a given set of conditions, only one will dominate and will be characterized by a unique combination of values for n, p and E_a. Thus the flow of ice over a broad range of conditions can be described by a composite "flow law" (e.g., Goldsby and Kohlstedt 2001):

$$\dot{\varepsilon} = \dot{\varepsilon}_{BD} + \dot{\varepsilon}_{VD} + \left(\frac{1}{\dot{\varepsilon}_{GBS}} + \frac{1}{\dot{\varepsilon}_{BS}}\right)^{-1} + \dot{\varepsilon}_{DC} \tag{7.3}$$

where each term is a power law of the form in Eq. 7.2 and the subscripts correspond to: *BD* for grain boundary diffusion (or Coble creep), *VD* for volume diffusion

(or Nabarro-Herring creep), *GBS* for grain-boundary sliding, *BS* for basal slip, and *DC* for dislocation creep.

The time dependent behavior of viscoelastic materials can be described by a *creep compliance J(t):*

$$J(t) = J_U + F(t) + \frac{t}{\eta_{ss}}, \tag{7.4}$$

where $J(0) \equiv J_U$ is defined as the unrelaxed compliance, which represents the immediate response to forcing, F(t) is some function of time (examples of which are described in Sect. 7.4.5) and η_{ss} is the steady-state viscosity.

Stress relaxation is the compliment to creep; it is the time dependent response to a fixed amount of strain that is applied instantaneously and held constant. The gradual decrease of stress that results is the stress relaxation function $M(t)$, from which is defined $M(0) \equiv M_U$, the unrelaxed modulus (Nowick and Berry 1972). Because there is a unique relationship between stress and strain, the relaxed modulus and compliance are reciprocal, i.e.,

$$M_R = \frac{1}{J_R}. \tag{7.5}$$

7.4.2 Stress–Strain Relationships in the Frequency Domain

The dynamic, or frequency-dependent, behavior of viscoelastic materials is described by the *complex compliance* $J^*(\omega)$ and the *complex modulus* $M^*(\omega)$. When a small periodic stress is applied, it follows the form $\sigma(t) = \sigma_0 \cos\omega t$, where angular frequency $\omega = 2\pi t$. In complex notation, this stress can be expressed as $\sigma^* = \sigma_0 e^{i\omega t}$ and the material response, by requirement of linearity, will be at the same frequency. The complex compliance, which is the ratio of periodic strain to stress, is related to the time domain response by transform according to:

$$J^*(\omega) = i\omega \int_0^\infty J(t) \exp(-i\omega t) dt \tag{7.6}$$

where $s = i\omega$ is the transform variable (e.g. Findley et al. 1976; Karato 2008). The complex compliance can also be written:

$$J^*(\omega) = \frac{\varepsilon_0}{\sigma_0} = J_1(\omega) - iJ_2(\omega) \tag{7.7}$$

where the real part, $J_1(\omega)$, is called the "storage compliance", and the imaginary part, $J_2(\omega)$, the "loss compliance" with:

$$\begin{cases} J_1(\omega) = J_U + \omega \int_0^\infty (J(t) - J_U) \sin \omega t dt \\ J_2(\omega) = -\omega \int_0^\infty (J(t) - J_U) \cos \omega t dt \end{cases} \tag{7.8}$$

Similarly, the c*omplex modulus* is defined as

$$M^*(\omega) = \frac{\sigma_0}{\varepsilon_0} = [J^*(\omega)]^{-1} = \left[J_1^2(\omega) + J_2^2\right]^{-\frac{1}{2}} \tag{7.9}$$

Since the periodic strain can be expressed as $\varepsilon^* = \varepsilon_0 e^{i(\omega t - \delta)} = J^*(\omega)\sigma_0 e^{i\omega t}$, then

$$\begin{gathered} J_1(\omega) = \frac{\varepsilon_0}{\sigma_0} \cos \delta \\ \text{and} \\ J_2(\omega) = \frac{\varepsilon_0}{\sigma_0} \sin \delta \end{gathered} \tag{7.10}$$

where δ is the phase lag between stress and strain, also known as the loss angle, and:

$$\tan \delta = \frac{J_2(\omega)}{J_1(\omega)} = \frac{M_2(\omega)}{M_1(\omega)}. \tag{7.11}$$

The real and imaginary parts of J^* and M^* are not independent but are related such that if either $J_1(\omega)$ or $J_2(\omega)$ (or either $M_1(\omega)$ or $M_2(\omega)$) is known for all frequency ranges (or at least for a very wide range), then the other can be calculated according to a mathematical property called the Kramers-Krönig relation.

7.4.3 Phase Lag and Attenuation

When the sinusoidally time-varying stress of a viscoelastic material is plotted against the sinusoidally time-varying strain of the same frequency, a hysteresis loop is formed, the dimensions of which represent various material properties (Fig. 7.5). The slope of the diagonal line bisecting the ellipse, for instance, is the absolute dynamic modulus $|M^*(\omega)|$. The area within the ellipse represents the energy per volume per cycle dissipated in the material, ΔW (e.g., Lakes 1999).

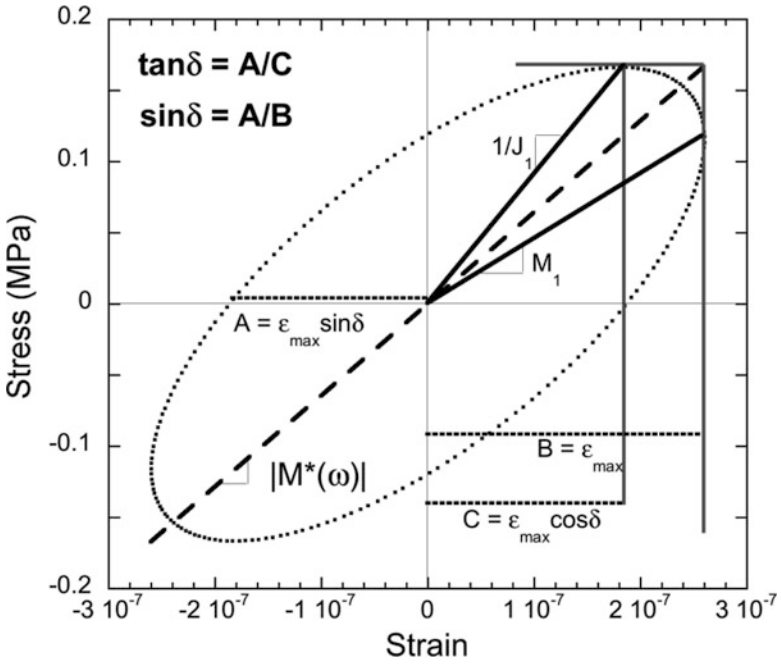

Fig. 7.5 Plot of cyclic stress versus cyclic strain, known as a Lissajous, or hysteresis loop. The dimensions of the elliptical loop provide values for various material properties (After Lakes 2004). In particular, the width of the figure is a measure of the phase lag δ, such that a purely elastic material would plot as a straight diagonal line with zero thickness. The figure shown here was generated using data from a particularly "lossy" material, ice + MS11 eutectic mixture, at 240 K and 0.1 Hz

The ratio of ΔW to the maximum elastic energy stored, W, for a given amplitude is equivalent to the inverse ratio of the real and imaginary parts of the complex compliance. According to the most commonly used definition, these ratios are related to the phase lag by:

$$\tan\delta = \frac{J_2}{J_1} = \frac{\Delta W}{2\pi W} = Q^{-1} \tag{7.12}$$

where Q is called the quality factor and its inverse is attenuation, the commonly adopted measure of damping in experimental studies (e.g., Nowick and Berry 1972; O'Connell and Budiansky 1978). However, it should be noted that within the context of tidal forcing, Eq. 7.12 assumes small dissipation. When considering a particularly lossy response, where phase lag is quite large, the simple relation of tanδ with Q^{-1} breaks down and a more precise definition should instead be employed (please see the Appendix of Efroimsky and Williams 2009 for a detailed derivation of Q^{-1}).

7.4.4 Simple Dissipation Models

A major goal of the research on material attenuation properties is to establish empirical relationships between quality factor and frequency. Such a relationship is important in order to extrapolate attenuation to conditions that cannot be probed by experimental techniques. This is especially relevant in the case of tidal forcing as it spans a frequency range from 10^{-4} down to 10^{-6} Hz (Fig. 7.1), which is difficult to obtain with existing techniques.

Many mechanical models have been proposed to describe material response. For purposes of visualization, these are often depicted as a collection of elastic springs and viscous dashpots, which, following the *Boltzmann superposition principal*, can be summed to represent an overall response. As previous researchers have admonished, however, these models should serve solely as a pedagogical device and are not truly representative of mechanical behavior (Lakes 1999; Cooper 2002).

A well-established method to evaluate mechanical behavior is to fit one of these models to a material's observed creep compliance $J(t)$. From this, the complex properties of $J^*(\omega)$ and $M^*(\omega)$ can be obtainable by application of the Laplace transform in Eq. 7.6. Here we present various phenomenological models of compliance that have been used, with varying degrees of success, to represent the mechanical response of a material to an applied stress. All of these models have known transforms tabulated in various references (e.g. Findley et al. 1976; Karato 2008). A review of the various relationships used in the literature on satellite dissipation can be found in Efroimsky and Lainey (2007) and Castillo-Rogez et al. (2011).

7.4.4.1 The Maxwell Model: Advantages and Limits

Most of the planetary studies on solid bodies have relied on the Maxwell model to describe dissipation. The Maxwell model (e.g., Maxwell 1867; Zschau 1978) offers the primary advantage that the phase lag can be expressed by two intrinsic properties: elasticity and viscosity. These two properties are represented in Fig. 7.6 by an ideal elastic spring (energy storage element) and a purely viscous dashpot (dissipation element). For a Maxwell model, the two elements are arranged in series. The single relaxation time represents the amount of time required for the energy stored in the spring to shift to and be dissipated by the dashpot. The real and imaginary components of the complex compliance for the Maxwell model are:

$$\begin{cases} J_1^{Max}(\omega) = \dfrac{1}{k} \\ J_2^{Max}(\omega) = \dfrac{1}{\eta\omega} \end{cases} \tag{7.13}$$

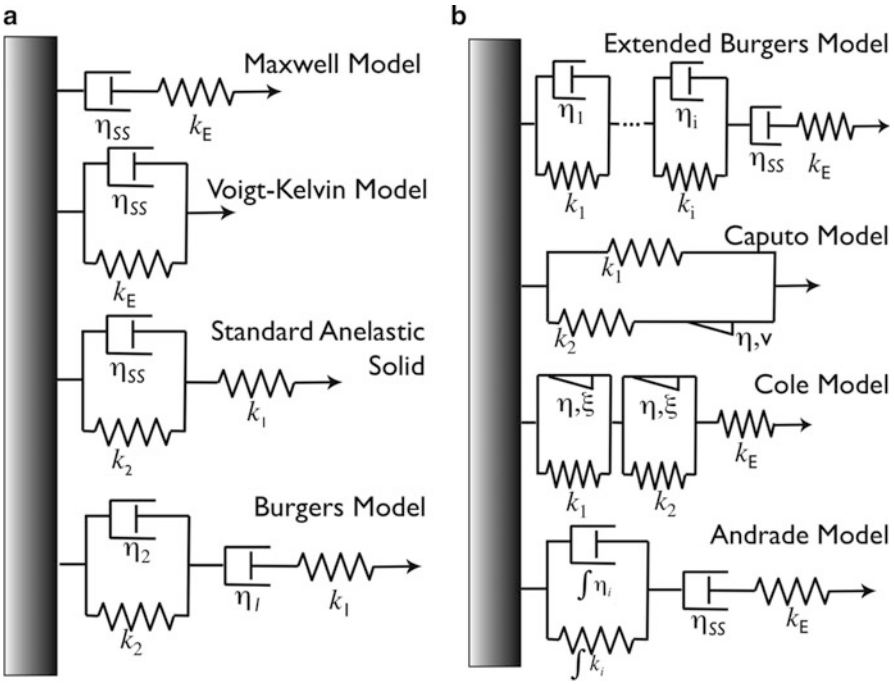

Fig. 7.6 Simple spring-and-dashpot models used to illustrate the components of various viscoelastic solid models, where a spring represents the elastic response, a dashpot the viscosity, and a spring-pot (triangle) is a fractional order response

As a result, it is possible to express the dependence of attenuation directly as a function of the angular frequency, so that $\tan\delta = k/\eta\omega \propto \omega^{-1}$.

A major historical reason that the Maxwell model has been the preferred model in planetary science is that it has relatively simple expressions for calculating attenuation and it renders reliable quantification of attenuation in some metals and rocks at high frequency (in the Hz to kHz range, e.g., Coyner and Randolph 1988). The Maxwell model has also been found to properly match the behavior of Earth's terrestrial material relaxed over long time scales, such as glacial rebound (e.g., Romanowicz 1994). More generally, the Maxwell model has been used to describe ice frequency-dependent anelasticity when forcing periods approximate the Maxwell time (e.g., Tobie et al. 2005 and references therein). However, the attenuation spectrum yielded by the Maxwell model significantly departs from experimental observations at frequencies greater than the Maxwell frequency.

The Maxwell model yields dissipation models that are infinitely large as temperature decreases. Simply put, the Maxwell model is not built to properly describe the mechanical properties of ice because it lacks a component accounting for anelasticity. However, the systematic application of the Maxwell model has been justified by the lack of comprehensive appreciation of ice anelasticity.

7.4.4.2 Voigt/Kelvin Model

Whereas a Maxwell model describes a spring and dashpot in mechanical series, the Voigt/Kelvin model takes those two elements and places them instead in mechanical parallel, so that both elements experience the same stress. When stress is first applied, the response is almost entirely viscous, but with time, the viscous element elongates and stress is gradually transferred to the elastic element. This model, often called delayed elasticity, does not contain a term for the initial elastic response on loading, nor does it contain a term for permanent plastic response. Thus, like the Maxwell model, by itself the Voigt/Kelvin model cannot describe the phenomenological behavior of viscoelastic materials over the full range of time.

7.4.5 Models Accounting for a Transient Creep Component

7.4.5.1 Standard Anelastic Solid

To closer approximate the response of solids, a three parameter mechanical model employs a Voigt/Kelvin unit in mechanical series with a single spring k_1 (Fig. 7.6a). This combination (also called a Zener model) describes an initial response entirely by k_1 at $t = 0$ followed by an anelastic response from the Voigt/Kelvin element. The corresponding real and imaginary parts obtained from inversion of *J(t)* are:

$$\begin{cases} J_1^{SAS}(\omega) = \dfrac{1}{k_1} + \dfrac{k_2}{k_2^2 + \eta^2\omega^2} \\ J_2^{SAS}(\omega) = \dfrac{\eta\omega}{k_2^2 + \eta^2\omega^2} \end{cases}. \tag{7.14}$$

Although the standard anelastic solid model can better approximate the transient response of solids, it has no viscous (non-recoverable) component and thus does not provide for a very long period response. Furthermore, its simplistic description of anelasticity relies on a single relaxation time. For that reason it has been found to be appropriate for representing attenuation due to proton reorientation and is commonly used in electrical studies, but it cannot account for complex microstructure of the material as do other models that include a broader range of relaxation times.

7.4.5.2 Burgers Model

The simplest mechanical model that captures all of the basic elements of material response is the Burgers or Four-element Model, which is created by placing a Maxwell unit and a Voigt/Kelvin unit in mechanical series (Fig. 7.6a). The creep

compliance for the Burgers model, then, is just the sum of the Maxwell and Voigt/Kelvin models:

$$J(t) = \frac{1}{k_1} + \frac{1}{k_2}\left[1 - \exp\left(\frac{-t}{\tau}\right)\right] + \frac{t}{\eta_{ss}} \tag{7.15}$$

where the three terms represent the elastic k_1, anelastic, and plastic η_{ss} responses, respectively, and τ is the relaxation time (e.g. Findley et al. 1976). Inversion of the Burgers model produces a Debye-type peak in the frequency domain, which is associated with the characteristic relaxation time of the Voigt/Kelvin element, superimposed onto the background attenuation of the Maxwell element. Thus the Burgers model, like the SAS model, describes attenuation in a material with only one relaxation time, whereas many materials have a far more complex response. For this reason, the Burgers model in its simple form is generally not used in geophysical applications (e.g., Jackson 1993; Jellinek and Brill 1956).

7.4.5.3 Extended Burgers Model

In order to reflect the complexity of planetary materials, some researchers replace the single relaxation time τ in the simple Burgers model with a suitably broad distribution $D(\tau)$ of relaxation times to more accurately describe the response in both the time and frequency domains (Tan et al. 2001; Jackson et al. 2004). The components of the complex compliance of this "extended" Burgers model are given by:

$$\begin{cases} J_1^{EB}(\omega) = \dfrac{1}{k_E}\left[1 + \Delta\displaystyle\int_0^\infty D(\tau)d\tau/(1+\omega^2\tau^2)\right] \\ J_2^{EB}(\omega) = \dfrac{\omega}{k_E}\Delta\displaystyle\int_0^\infty \tau D(\tau)/(1+\omega^2\tau^2) + \dfrac{1}{\eta_{ss}\omega} \end{cases}, \tag{7.16}$$

where the parameter Δ is anelastic relaxation strength, which is a direct function of the concentration, mobility and geometry of the defect(s) accommodating the relaxation (Jackson et al. 2002). Expressions of Δ for various deformation mechanisms can be found in Karato and Spetzler (1990). $D(\tau)$ is a function representing the distribution of relaxation times characterizing the broad plateau in the frequency dependence of Q^{-1}:

$$D(\tau) = \frac{\alpha\tau^{-(1-\alpha)}H(\tau - \tau_m)H(\tau_M - \tau)}{\tau_M^\alpha - \tau_m^\alpha} \tag{7.17}$$

where H is the Heaviside step function, τ_M and τ_m bound the absorption band in which the frequency-dependence of the dissipation factor is characterized by a slope α (positive and lower than 1). Inversion of the Extended Burgers model has been found to fit laboratory spectra of rocky material in frequency range $1–10^{-3}$ Hz (e.g., Tan et al. 2001; Jackson et al. 2002).

7.4.5.4 Caputo Model

Another model that seeks to describe the weak frequency dependence observed over a wide frequency range is the Caputo model (Caputo 1966, 1967; Minster and Anderson 1981). The Caputo body improves upon the SAS model by employing a special stress-strain relation that has a memory mechanism in the form of a fractional derivative and a long-time scale transient creep. For this purpose, the model replaces a dashpot with a *spring-pot*, which relies on viscosity and a scaling term v, such that the spring-pot has an intermediate order $1 > v > 0$ between pure elastic and pure viscous behavior (Fig. 7.6b). The storage and loss components of the Caputo model are:

$$\begin{cases} J_1^{Ca} = \dfrac{k_2 - k_1}{k_1 k_2} \omega^v \sin(v\pi/2) \\ J_2^{Ca} = \left[1 + \dfrac{\omega^v}{k_1 k_2} + \omega^v \dfrac{(k_1 + k_2)}{k_1 k_2} \cos(v\pi/2) \right] \end{cases} \tag{7.18}$$

where k_1 and k_2 are functions of the elasticity of the material.

Although the Caputo model proved to describe well the attenuation associated with Earth's free oscillations and torsional modes (Caputo and Mainardi 1979), it is generally deemed to have limited applicability (e.g., Bagdassarov 1999; Han et al. 2007) and is rarely used in the planetary science literature (e.g., Wieczerkowski and Wolff 19981998). However, the observation that Q can come close to a constant over a wide frequency range has been extensively used in planetary models developed in the 1970s and 1980s, so we provide this model for reference (see Sect. 7.5).

7.4.5.5 Cole Model

This model was introduced by Cole (1995) in order to quantify the experimental observations of attenuation in saline ice and isolate the relaxation due to dislocation motion (Cole and Durell 1995). As such, it is the only model developed specifically to characterize the response of ice. Like the Extended Burgers model, the Cole model seeks to explain the broad attenuation plateau and also the low-frequency modulus asymptote observed in the experimental data. In this case, the Debye-peak producing Voigt/Kelvin element is replaced with an adjustable parameter ξ to control the peak width while keeping its area constant (e.g., $\xi = 1$ for a Debye peak). The storage and loss components of the dislocation-dominated compliance of the Cole model are:

$$\begin{cases} J_1^{Cole} = \dfrac{1}{k_E} + \delta D \left[1 - \dfrac{2}{\pi} \tan^{-1}(\exp(\xi s)) \right] \\ J_2^{Cole} = \xi \delta D \dfrac{1}{\exp(\xi s) + \exp(-\xi s)} \end{cases} \tag{7.19}$$

where the quantity $\delta D = \rho\Omega b^2/\sigma_r$ and $s = \ln(\tau_C\omega)$. The Cole model is based on the theory of oscillatory motion of basal plane dislocations (e.g., Weertman 1955; 1983; see also Sect. 7.2.4) and thus uses the mobile dislocation density ρ, the length of the Burgers vector b, and the restoring stress constant σ_r, which is the force the dislocation segment "feels" in its Peierls potential trough. The orientation factor Ω is a geometry term related to the degree of alignment between ice grains. The model was further developed by Cole (1995) and Cole and Durell (2001), to describe relaxation by grain boundary sliding and to include the effect of strain history, salinity and porosity as they are incorporated into ρ and Ω. Cole and his collaborators demonstrated the applicability of the model to describe the anelastic response of natural and laboratory grown ice. However, its ability to model the response of ice at frequencies of planetary significance is questionable. At the very low frequencies of tidal forcing, viscoelasticity, *in addition to* anelasticy, is expected to be responsible for relaxation (e.g. Karato and Spetzer 1990). Unlike the Extended Burgers model, the Cole model provides no term for low frequency viscous relaxation. Another limitation is that the model uses a fixed value for the parameter ξ that is only based on fittings to empirical data so that alterations based on the context and nature of the microstructure cannot be made. Still, the wealth of data collected by that group is significant and the Cole model's ability to isolate and model the dislocation-based dissipation mechanism in ice is significant.

7.4.5.6 Andrade Model

The Andrade creep function was introduced by Andrade (1910) to describe transient creep in metals. In its initial form, it was expressed as:

$$J(t) = \frac{1}{\mu} + \beta t^m. \tag{7.20}$$

The full form of the Andrade creep function as applied to ice was introduced by Duval (1976, 1978):

$$J(t) = \frac{1}{k_E} + \beta t^m + \frac{t}{\eta_{ss}} \tag{7.21}$$

where β is a constant determined by the properties of the defects driving attenuation (i.e., their density and mobility) and, as such, that parameter is a direct function of the viscosity of the material (Castillo-Rogez et al. 2011). Shown in Fig. 7.6b, the transient element βt^m represents an infinite number of Voigt/Kelvin elements possessing a continuous distribution of relaxation times (Andrade 1910; Duval et al. 1983; Cooper 2002). The parameter m has been measured for a variety of materials, including polycrystalline ice (Ladanyi and Saint-Pierre 1978; McCarthy et al. 2007) and monocrystalline ice (Castillo-Rogez et al. 2011), and is generally

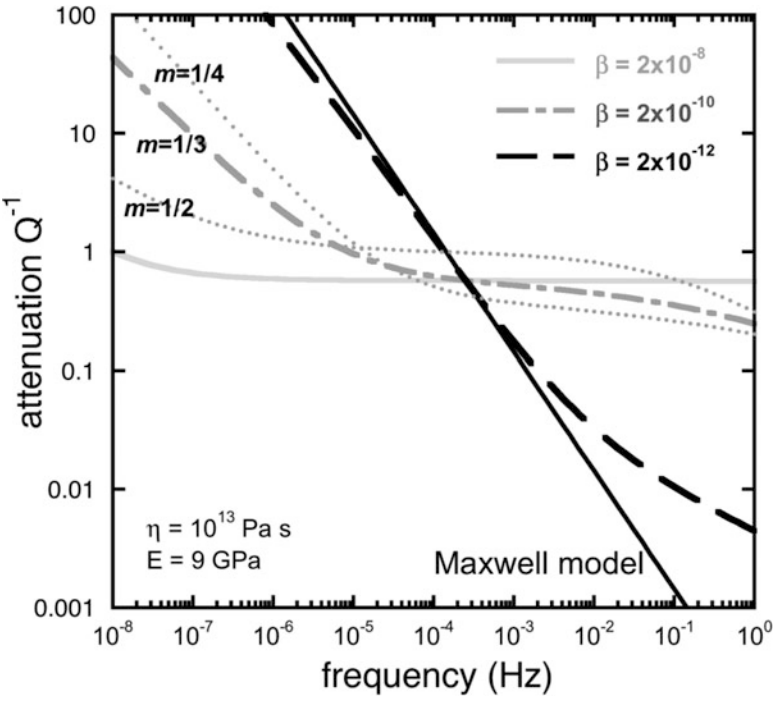

Fig. 7.7 A comparison of the Andrade-based model to the Maxwell model. The various lined curves represent different listed values for the parameter of β (while assuming constant $m = 1/3$). The *dotted lines* represent the effect of changing m (while keeping constant $\beta = 2 \times 10^{-10}$). Only at very small β does the Andrade-based model transition toward the Maxwell model

found to be between 1/3 and 2/3 (cf. Weertman and Weertman 1975). The dependence of m on experimental conditions or material properties is not clear. In the case of silicates, it has been suggested that the value of m is primarily determined by the lack of uniformity in grain shapes and the presence of impurities (e.g., Lee and Morris 2010). When the Andrade creep function is transformed, the storage and loss components are:

$$J_1^{And}(\omega) = \frac{1}{k_E} + \beta\Gamma(1+m)\omega^{-m}\cos\left(\frac{m\pi}{2}\right)$$
$$J_2^{And}(\omega) = \beta\Gamma(1+m)\omega^{-m}\sin\left(\frac{m\pi}{2}\right) + \frac{1}{\eta_{ss}\omega}, \tag{7.22}$$

where $\Gamma(m + 1)$ is the gamma function. The spectra predicted by the Andrade creep function is such that at very low frequencies, $Q^{-1} \propto f^{-(1-m)}$ and the slope of the intermediate band (i.e. the α-term of the Extended Burgers model) can be any value between 0 and $-(1-m)$. The length, slope and location in frequency space of the band are determined by the relative magnitudes of modulus, viscosity and β (Fig. 7.7).

A point worth noting about this model is that at frequencies lower than the Maxwell frequency (where viscoelastic theory predicts anelastic behavior to end and purely viscous behavior to dominate), the model can continue to have a moderate slope. This may be an indication that a mathematical model based on the Andrade creep function loses physical meaning at very low frequency. However, the fact that no experimental studies on planetary materials have yet demonstrated the predicted sharp transition to purely viscous behavior (a slope of -1 in log-log plot) may instead suggest that real materials continue to sample additional anelastic mechanisms beyond the Maxwell frequency. The degree of departure from the Maxwell model has been proposed to be a function of the value of β (Castillo-Rogez et al. 2011) As shown in Fig. 7.7, if beta is small (e.g., $\sim 10^{-12}$ as found in olivine; Jackson et al. 2002), then the attenuation spectrum approaches that predicted for a Maxwell model. On the other hand, the larger the value of β, due to increased defect density, the greater departure is to be expected.

7.5 Applications to Solar System Objects

The effect of tidal stress in outer planet satellites plays a major role in the geophysical, geological, and orbital evolution of these objects. Orbital evolution and tidal heating depend on the tidal Love number h_2, which expresses the amplitude of deformation in response to the tidal potential and the friction coefficient Q^{-1}.

7.5.1 Historical Approach to Tidal Dissipation Modeling in Planetary Satellites

Many studies over the past five decades have assumed that icy monoliths are characterized by a dissipation factor on the order of 100. That suggestion was based on available acoustic measurements, which also showed that the dissipation factor of ice and rock was frequency independent at ultrasonic frequency (Knopoff 1964; Goldreich and Soter 1966). Peale et al. (1980) justified a value of Q equal to 100 based on measurements obtained on ice by Nakamura and Abe (1980). However, the latter measurements were performed at seismic frequencies. Still, that rough estimate proved consistent in modeling the orbital evolution of Saturn's satellite Mimas from the synchronous orbit to its present location (Goldreich and Soter 1966). A value of $Q = 100$ has also been used for representing the dissipation factor of very porous bodies (e.g., Phobos, Yoder 1982; binary asteroids, Margot et al. 2002), as a step toward inferring the rigidity of these objects.

However, the assumption that ice dissipation factor is not frequency-dependent and equal to 100 finds its limit when modeling satellites large enough to have undergone some internal evolution. For example, Peale (1986) noted that in such a framework, it

is not possible to explain the spin-orbit resonance of Saturn's satellite Iapetus (see discussion in Sect. 7.5.5). Nor is it adequate to explain the intense heating measured on Enceladus (Spencer et al. 2006), which is believed to be due in large part to tidal heating. Although a few recent studies have used such an assumption (e.g., Meyer and Wisdom 2007), most of the satellite dissipation studies developed since the mid-1980s have relied on the application of a Maxwell solid model to approximate Q at satellite forcing frequencies. That approach has shaped our understanding of icy satellite thermal and orbital evolution for the past two decades (Sect. 7.5.2). As described above, despite its convenience, the Maxwell model fails to account for planetary material anelasticity, which may be the main attenuation mechanism expressed at the forcing frequencies relevant to satellite tides. A few studies have also attempted to compare the dissipation obtained from various models: Maxwell body, Caputo model, SAS, and Burgers model (e.g., Wieczerkowski and Wolf 1998; Hussmann and Spohn 2004; Robuchon et al. 2010). However, the latter models fail to describe the full range of viscoelastic behavior.

A novel approach to the problem is emerging, starting with the introduction of the Andrade-based model as potentially a better approach for describing planetary ice attenuation properties by McCarthy et al. (2007) and with its first application to modeling of Enceladus' tidal response by Rambaux et al. (2010). However, as noted by Castillo-Rogez et al. (2011), the lossy nature of polycrystalline ice requires that care must be taken in the application of laboratory attenuation data (which is expressed as the tangent of the phase lag) to models of tidal torque (which utilize the sine of phase lag) (Goldreich and Peale 1966; Efroimsky and Williams 2009). The approximation of $\sin \delta \sim \tan \delta = Q^{-1}$ that is often used for materials with Q greater than 10 will not hold with highly dissipative materials such as ice. We refer readers to Efroimsky and Williams (2009) and Tobie et al. (2005) for details on the calculation of torque and of the tidal response of icy bodies.

7.5.2 *Mechanisms Driving Dissipation in Icy Satellites*

Similar to that discussed in Sect. 7.4, the mechanisms in the viscoelastic regime that drive dissipation in solid bodies also depend on the nature, density, and mobility of defects, which are functions of temperature, stress, grain size, and impurity content. The dominant creep mechanisms expected in pure water ice can be mapped as a function of stress and grain size (Fig. 7.8 after Goodman et al. 1981; Goldsby and Kohlstedt 2001). That map shows that in most satellites, tidal stress is on the order of a few hundred or thousand Pascal, such that tidal stress is primarily accommodated by the diffusion of defects within the lattice. A few objects are subject to greater tidal stress peak amplitudes: the Galilean satellite Europa, the Kronian satellites Enceladus, and Uranus' Mimas, Ariel and Miranda. With the exception of Mimas, these satellites share the characteristic of having recently been geologically active (and possibly still active) as evidenced by their complete lack of large craters.

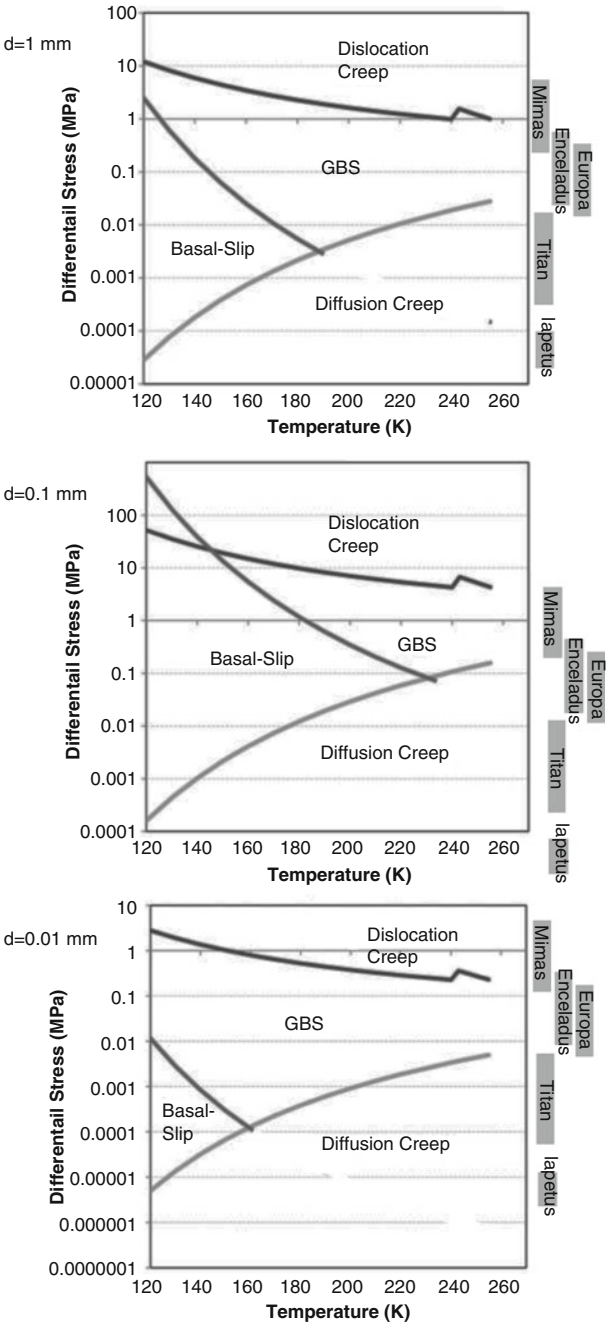

Fig. 7.8 Deformation mechanisms preferentially expressed in ice as a function of stress and temperature conditions, and for different grain sizes (assuming homogeneous grain size). The right-hand column shows the range of cyclic peak stress amplitudes expected in various icy satellites (see Fig. 7.1). This figure is built after the approach presented in Barr and Pappalardo (2005) using input parameters to Eq. 7.2 taken from Goldsby and Kohlstedt (2001). The mechanisms expected to accommodate stress are dislocation creep, dislocation-accommodated grain-boundary sliding (GBS), basal-slip accommodated grain-boundary sliding, and diffusion creep

The role of tidal heating in preserving a deep ocean in Europa and promoting intense geological activity on Enceladus is a topic of primary interest as these objects are the current target of the ongoing *Cassini-Huygens* Mission and the prospective *Europa and Jupiter System Mission*. It has been suggested that the tidal strain in icy satellites is so small that the response of the object is non-linear (Montagnat and Duval 2004). The situation may be different in the case of Enceladus and Europa, subject to stresses greater than 0.1 MPa and possible stress concentration, as suggested by the model of Tobie et al. (2008).

Also, satellites' orbital properties have evolved as a consequence of the tides they are subject to and the tides they exert on their primaries. It is expected that, in their early history, outer planet satellites were closer to their primaries (e.g., Zhang and Nimmo 2009), had higher eccentricity, and possibly possessed deep oceans. Thus, at least for a short period of time, they could have undergone significant tidal stress and increased tidal heating.

7.5.3 Key Results from the Maxwell Body Approximation

Since the unrelaxed modulus of ice shows little dependence on temperature for the conditions encountered in icy satellites (Parameswaran 1987), the attenuation spectrum predicted by the Maxwell model mostly depends on the viscosity of the material. In the frame of the Maxwell model, there is an important coupling between internal friction and the occurrence of convective heat transfer through the viscosity of the material. In other words, if the conditions (temperature, grain size) are such that material defects can easily move, then they can also be involved in anelastic dissipation. This observation is at the origin of numerous studies that have highlighted convective regions in icy satellites as preferential regions for tidal heating (e.g., Sotin et al. 2002; Fig. 7.9).

In this framework, tidal dissipation reaches a peak when the Maxwell time of the material, i.e., the ratio of its viscosity to elastic modulus, equals the tidal forcing period (e.g., the orbital period in the case of satellites in spin-orbit resonance). In this context, tidal dissipation is a runaway phenomenon. It contributes to increasing the temperature and, thus, decreasing the material viscosity, which then promotes further dissipation. However, if the viscosity becomes too low and the ice volume too small, the tidal dissipation becomes less efficient, and the ice starts cooling down. The threshold between the two trends is determined by the Maxwell time of the dissipative material. Tidal dissipation is in steady-state if that property is equal to the forcing period. The consequent interplay between the thermal and orbital states of planetary satellites was integrated in detailed geophysical models by Hussmann and Spohn (2004). These authors suggested that Europa and Io have been the probable objects of oscillatory phases of runaway heating and cooling associated with large changes in orbital eccentricity, alternating with quasi-steady state periods. They also demonstrated that departure from the equilibrium

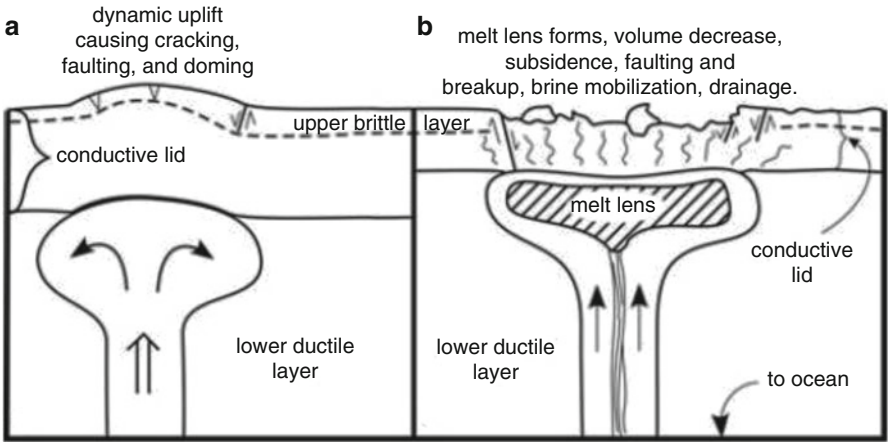

Fig. 7.9 Illustration of the impact of tidal dissipation on the geological activity of Europa driven by convective upwelling (Reprinted with authorization from the American Geophysical Union)

state is transitory, as the satellites tend to rapidly return to equilibrium. At present, most satellites, except Enceladus (Meyer and Wisdom 2008), should be at or close to equilibrium.

7.5.4 Impact of Anelasticity on the Tidal Response of Icy Satellites

Recent studies have suggested that an Andrade-based model may be more appropriate to the modeling of satellite tidal response than the Maxwell model (e.g., Nimmo 2008; Roberts and Nimmo 2008). At the time of this chapter's preparation, a few studies have been working with a complex compliance based on the Andrade creep model in geophysical modeling of icy satellites (e.g., Rambaux et al. 2010). Castillo-Rogez et al. (2011) have attempted to develop a hybrid model that combines (a) at high frequency: the distribution of characteristic times in the anelastic regime, as formulated in the Andrade model, and (b) at low frequency: a purely viscous response expressed with the Maxwell body. The transitional region between the purely anelastic and viscous regimes is not well understood and needs to be further studied in laboratory.

The theoretical attenuation spectrum presented in Fig. 7.10 features a strong change in the frequency dependence of attenuation around the inverse of the Maxwell time. That threshold is a function of the mechanism involved in the dissipation. Since ice viscosity shows a strong dependence on temperature, $1/\tau$ is commonly outside the range of forcing frequencies relevant to satellite tides. Taking Enceladus as an example, for an ice shear modulus of 3.3 GPa (e.g., Parameswaran 1987), τ equals the orbital period for a viscosity of ~4×10^{14} Pas.

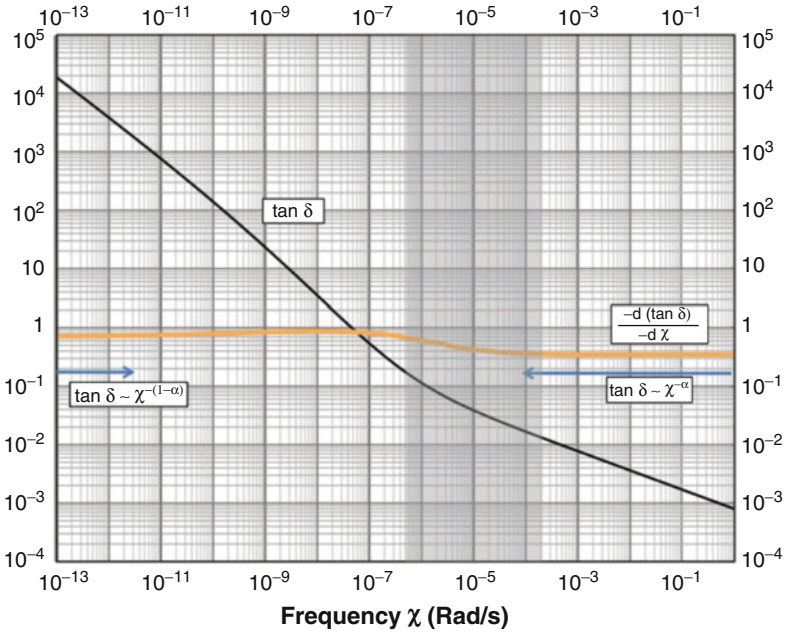

Fig. 7.10 Examples of attenuation spectra for the Andrade model for $\alpha = 0.5$ and $\beta = 5 \times 10^{-13}$

This means that material with larger viscosity will be dominated by the anelastic response, whereas warmer material may be dominated by purely viscous behavior and thus well approximated by a Maxwell solid model. However, in general, the frequency range of direct interest to icy satellite modeling coincides with anelastic-dominated behavior. If the icy satellites accreted cold (e.g., Ellsworth and Schubert 1983; Matson et al. 2009), their dissipative behavior must have been primarily governed by their material anelasticity (until the contribution of viscosity became increasingly significant as a consequence of satellite warming). In such conditions the material is expected to be more dissipative than that modeled with a Maxwell solid model. Related to that issue, the evolving tidal forcing amplitudes and frequencies resulting from the inward/outward evolution of the satellites orbits (e.g., Meyer and Wisdom 2007; Zhang and Nimmo 2009) must have also affected the style of attenuation in these objects. To illustrate these considerations, the dissipation factor for a homogeneous ice sphere is plotted as a function of period and viscosity in Fig. 7.11 in the frame of the Maxwell body (Fig. 7.11a) and Andrade-based model (Fig. 7.11b). Both approaches yield a maximum of dissipation as the Maxwell time of the material and the tidal period coincide. At low viscosities, both models tend to overlap. However, the departure of the Maxwell body from the Andrade-based model increases for increasing ice viscosities and decreasing forcing periods. The significance of that change in approach to modeling the geophysical and dynamical evolution of planetary satellites remains to be evaluated.

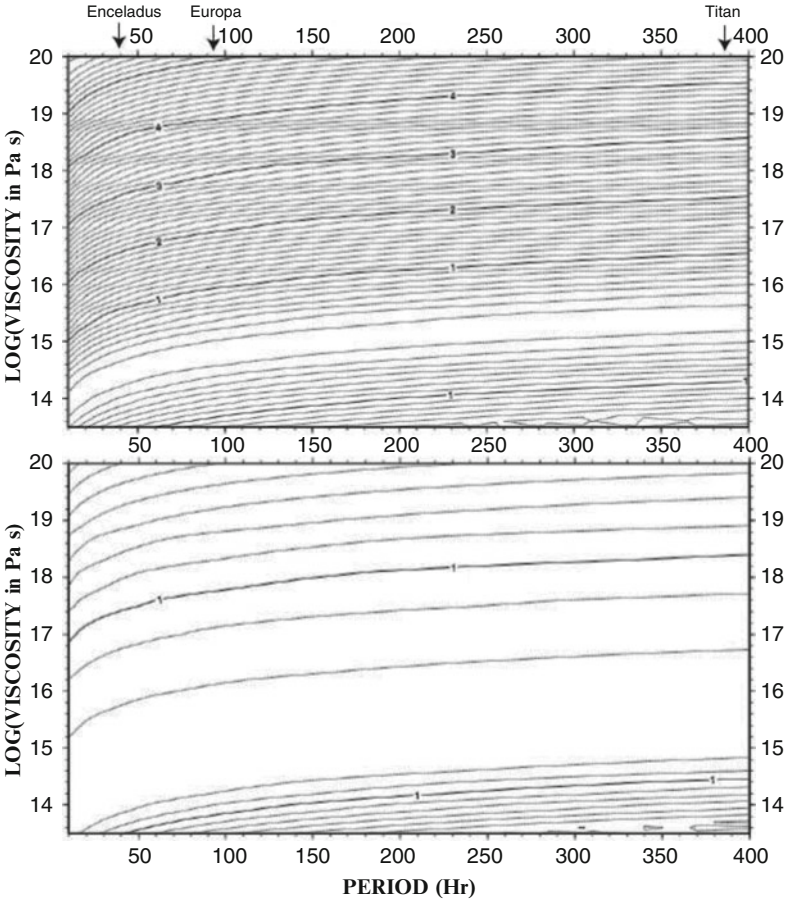

Fig. 7.11 Decimal logarithm of the quality factor Q for a homogeneous sphere of pure water ice as a function of viscosity and forcing period (see Castillo-Rogez et al. (2011) for details about the calculation of these figures). *Top*: for the Maxwell model; *Bottom*: for the Andrade creep function assuming a parameter α equal to 0.3

7.5.5 Application: Iapetus' Evolution to Spin-Orbit Resonance

Due to its unusual orbital and geological properties, the Saturnian satellite Iapetus has been the focus of several recent studies aimed at modeling its despinning to synchronous rotation. Peale (1986) pointed out the apparent inconsistency between Iapetus' synchronous rotation and the dissipative properties assumed at the time. Using a dissipation factor equal to 100, Peale et al. (1979) inferred a despinning timescale of 14 Gy for Iapetus. From coupling thermal and dynamical evolution, Castillo-Rogez et al. (2007) suggested that Iapetus could achieve despinning on a shorter timescale, on the order of 1 Gy. However, that study relied on the Maxwell

model, such that the temperature had to reach the water ice melting point for despinning to become significant and complete in a few thousand years. That scenario was found to be problematic because solid-state convection was ignored. As described above, due to the strong coupling between attenuation and viscosity, significant tidal dissipation implies that the material can deform in a way suitable to promote convective heat transfer. Such a possibility was demonstrated in the case of Iapetus with the application of a Four-Element model (Burgers) to account for the transient properties of the material (Robuchon et al. 2010). However, that study fully decoupled transient and steady-state creep, which is inconsistent with experimental observations and theoretical considerations. The most recent take on the topic was to apply an Andrade-based model using an empirical relationship between the Andrade parameter β and the steady-state creep (Castillo-Rogez et al. 2011). In such a framework, convection and tidal dissipation are still coupled, but to a lesser extent (to the power of the Andrade parameter α). As a result, these authors found geophysical models in which convection onset and tidal dissipation were not mutually exclusive.

7.6 Conclusions and Roadmap for Future Research

We have reviewed the state of knowledge of ice attenuation properties as of 2010. At this time, the identification of ice mechanical properties over a range of forcing frequencies relevant to the tides of icy satellites is in progress. There seems to be a general understanding in the recent literature that the simple Maxwell model may not be suited to describing the tidal response of icy satellites. At this stage, there is no definitive answer as to which alternative model is best, especially between the Andrade-based and the Extended Burgers models, for describing the response of planetary materials over a wide range of frequencies encompassing satellite tides.

There is a good chance that in the next decade, significant advances from an experimental and theoretical point of view will lead to a better understanding of attenuation in icy materials as there is a strong interest in that research to support ongoing and prospective missions to icy bodies: e.g., *New Horizons* Mission to Pluto and Charon, *Dawn* Mission to Ceres, etc.

As discussed above, attenuation can be quantified as a function of material defect properties. The challenge posed to future geophysical models is to progress from using "black-box" input parameters to considering the material's thermal history, from accretion or freezing from a deep salty ocean, to its possible upwelling to the surface as a consequence of solid-state convection. Processes of importance include defect annealing (e.g., recrystallization), the role played by tidal stress in keeping the grain size small, and the segregation of impurities.

Future research should focus on a variety of frozen volatile compositions, including: ammonia hydrates, clathrate hydrates, and hydrated salts, as well as mixtures of ice and silicates. The importance of focusing on multiphase compositions is not limited to the problems addressed in this study but is also relevant to a more general

understanding of planetary material mechanical properties with geological and geophysical applications (Castillo-Rogez et al. 2009).

Aside from composition, the impact of microstructure and its evolution as a result of thermal and mechanical aging require dedicated studies. Although the role of impurities in preventing grain growth has become an important feature of recent models, the actual impact on material microphysics remains to be implemented.

Most satellites experience tidal stresses at least one order of magnitude smaller than the stresses currently achieved by laboratory experiment. Proper extrapolation to planetary conditions requires a more detailed knowledge of the mechanisms controlling dissipation and the conditions under which the response becomes non-linear. There is also a need to better characterize how tidal stress affects the stress distribution in icy satellites, and especially how tidal and convective straining interact and influence one another. Of crucial importance, attenuation under pure shear conditions has to be properly characterized in order to develop geophysical models approaching as closely as possible the conditions expected in icy satellites.

Acknowledgements We would like to thank several people for discussions that contributed to this chapter, including Reid Cooper and Yasuko Takei. The authors would also like to thank Shun Karato and Michael Efroimsky for their thorough reviews. Part of this review chapter was prepared at the Jet Propulsion Laboratory, California Institute of Technology, under contract with NASA.

References

Ahmad S, Whitworth RW (1988) Dislocation motion in ice: a study by synchrotron X-ray topography. Philos Mag A 57(5):749–766

Aksnes K, Franklin FA (2001) Secular acceleration of Io derived from mutual satellite events. Astron J 122:2734–2739. doi:10.1086/323708

Andrade END (1910) On the viscous flow in metals and allied phenomena. Proc R Soc Lond Ser-A 84:1–12

Ashby MF, Verrall RA (1973) Diffusion-accommodated flow and superplasticity. Acta Metall Mater 21:149–163. doi:10.1016/0001-6160(73)90057-6

Bagdassarov NS (1999) Viscoelastic behavior of mica-based glass-ceramic aggregate. Phys Chem Miner 26:513–520

Baker I (1997) Observation of dislocations in ice. J Phys Chem B 101:6158–6162

Barnhoorn A, Jackson I, Fitz Gerald JD, Aizawa Y (2007) Suppression of elastically accommodated grain-boundary sliding in high-purity MgO. J Eur Ceram Soc 27:4697–4703

Barr AC, Milkovich SM (2008) Ice grain size and the rheology of the Martian polar deposits. Icarus 194:513–518. doi:10.1016/j.icarus.2007.11.018

Barr AC, Pappalardo RT (2005) Onset of convection in the icy Galilean satellites: influence of rheology. J Geophys Res 110:E12005. doi:10.1029/2004JE002371

Beeman ML, Kohlstedt DL (1993) Deformation of fine-grained aggregates of olivine plus melt at high temperatures and pressures. J Geophys Res 98(4):6443–6452

Bjerrum N (1952) Structure and properties of ice I. Science 115(2989):385–390

Brill R, Camp PR (1961) Properties of ice. Research report no 68 of the SIPRE snow, ice, and permafrost research establishment. US Army Terrestrial Science Center, Hanover

Buechner PM, Stone D, Lakes RS (1999) Viscoelastic behavior of superplastic 37 wt% Pb 63 wt% Sn over a wide range of frequency and time. Scr Mater 41(5):561–567
Burdett CF, Queen TJ (1970) The role of dislocations in damping. Metall Rev 143(1):65–78
Caputo M (1966) Linear models of dissipation whose Q is almost frequency independent. Ann Geophys 19:383–393
Caputo M (1967) Linear models of dissipation whose Q is almost frequency independent – II. Geophys J R Astron Soc 13:529–539
Caputo M, Mainardi F (1979) A new dissipation model based on memory mechanism. Pure Appl Geophys 91(1):134–147
Castelnau O, Duval P, Montagnat M, Brenner R (2008) Elastoviscoplastic micromechanical modeling of the transient creep of ice. J Geophys Res 113:B11203. doi:10.1029/2008JB005751
Castillo JC, Mocquet A, Sotin C (2000) Détecter la présence d'un océan dans Europe à partir de mesures altimétriques et gravimétriques. CR Acad Sci IIA-Earth Planet Sci 330:659–666
Castillo-Rogez J, Matson DL, Sotin C, Johnson TV, Lunine JI, Thomas PC (2007) Iapetus' geophysics: rotation rate, shape, and equatorial ridge. Icarus. doi:10.1016/j.icarus.2007.02.018
Castillo-Rogez JC, Durham WB et al (2009) Laboratory studies in support of planetary geophysics. White paper to the decadal survey solar system 2012
Castillo-Rogez JC, Efroimsky M, Lainey V (2011) The tidal history of Iapetus. Dissipative spin dynamics in the light of a refined geophysical model. J Geophys Res 116:E09008. doi:10.1029/2010JE003664
Cochran ES, Vidale JE, Tanaka S (2004) Earth tides can trigger shallow thrust fault earthquakes. Science 306:1164–1166. doi:10.1126/science.1103961
Cole DM (1995) A model for the anelastic straining of saline ice subjected to cyclic loading. Philos Mag A 72(1):231–248
Cole DM (2001) The microstructure of ice and its influence on mechanical properties. Eng Fract Mech 68:1797–1822
Cole DM, Durell GD (1995) The cyclic loading of saline ice. Philos Mag A 72(1):209–229
Cole DM, Durell GD (2001) A dislocation-based analysis of strain-history effects in ice. Philos Mag A 81(7):1849–1872
Cole DM, Johnson RA, Durell GD (1998) Cyclic loading and creep response of aligned first-year sea ice. J Geophys Res 103(C10):21, 751-21,758
Cooper RF (2002) Seismic wave attenuation: energy dissipation in viscoelastic crystalline solids. In: Karato S, Wenk HR (eds) Plastic deformation of minerals and rocks, vol 51, Reviews in mineralogy and geochemistry. Mineralogical Society of America, Washington, DC, pp 253–290
Cooper RF, Kohlstedt DL (1984) Rheology and structure of olivine-basalt partial melts. J Geophys Res 91(B9):9315–9324
Coyner KB, Randolph RJ (1988) Frequency-dependent attenuation in rocks. Technical report A672502
Dash JG, Rempel AW, Wettlaufer JS (2006) The physics of premelted ice and its geophysical consequences. Rev Mod Phys 78:695
Durham WB, Stern LA (2001) Rheological properties of water ice – applications to satellites of the outer planets. Annu Rev Earth Planet Sci 29:295–330
Durham WB, Pathare AV, Stern LA, Lendferink HJ (2009) Mobility of icy sand packs, with application to Martian permafrost. Geophys Res Lett 36:L23203
Duval P (1976) Temporary or permanent creep laws of polycrystalline ice for different stress conditions. Ann Geophys 32:335–350
Duval P (1978) Anelastic behaviour of polycrystalline ice. J Glaciol 21(85):621–628
Duval P, Ashby MF, Anderman I (1983) Rate-controlling processes in the creep of polycrystalline ice. J Phys Chem 87:4066–4074
Efroimsky M, Lainey V (2007) On the theory of bodily tides. In: Belbruno E (ed) New trends in astrodynamics and applications III. American Institute of Physics, Melville, pp 131–138
Efroimsky M, Williams JG (2009) Tidal torques. A critical review of some techniques. Celest Mech Dynam Astr 104:257–289, arXiv:0803.3299 1230

Ellsworth K, Schubert G (1983) Saturn's icy satellites: thermal and structural models. Icarus 54:490–510
Faul UH, Jackson I (2005) The seismological signature of temperature and grain size variations in the upper mantle. Earth Planet Sci Lett 234:119–134
Faul UH, FitzGerald JD, Jackson I (2004) Shear wave attenuation and dispersion in melt-bearing olivine polycrystals: 1. Microstructural interpretation and seismological implications. J Geophys Res 109:B06202
Findley WN, Lai JS, Onaran K (1976) Creep and relaxation of nonlinear viscoelastic materials. Dover, New York
Fountaine FR, Ildefonse B, Bagdassarov NS (2005) Temperature dependence of shear wave attenuation in partially molten gabbronorite at seismic frequencies. Geophys J Int 163:1025–1038
Friedson AJ, Stevenson DJ (1983) Viscosity of rock-ice mixtures and applications to the evolution of icy satellites. Icarus 56(1):1–14
Fukuda A, Hondoh T, Higashi A (1987) Dislocation mechanisms of plastic deformation in ice. J Phys C 48(3):163–173
Goldreich P, Peale S (1966) Spin-orbit coupling in the Solar system. Astron J 71:425–438
Goldreich P, Sari R (2009) Tidal evolution of rubble piles. Astrophys J 691:54
Goldreich P, Soter S (1966) Q in the Solar system. Icarus 5:375–389
Goldsby DL (2007) Diffusion creep of ice: constraints from laboratory creep experiments. LPS 38:2186
Goldsby DL, Kohlstedt DL (2001) Superplastic deformation of ice: experimental observations. J Geophys Res-Solid Earth 106:B11017–B11030. doi:10.1029/2000JB900336
Goodman DJ, Frost HJ, Ashby MF (1977) The effect of impurities on the creep of ice Ih and its illustration by the construction of deformation maps, isotopes and impurities in snow and ice. Int Assoc Sci Hydrol, Int Union Geod Geophys 118:29–33, IASH Publication
Goodman DJ, Frost HJ, Ashby MF (1981) The plasticity of polycrystalline ice. Philos Mag A 43:665–695
Granato AV, Lücke K (1956) Theory of mechanical damping due to dislocations. J Appl Phys 27:582
Greenberg R, Geissler P, Hoppa G, Tufts BR, Durda DD, Pappalardo R, Head JW, Greeley R, Sullivan R, Carr MH (1998) Tectonic processes on Europa: tidal stresses, mechanical response, and visible features. Icarus 135:64–78
Gribb TT, Cooper RF (1998) Low-frequency shear attenuation in polycrystalline olivine: grain boundary diffusion and the physical significance of the Andrade model for viscoelastic rheology. J Geophys Res 103:B11, 27, 267–27, 279
Gribb TT, Cooper RF (2000) The effect of an equilibrated melt phase on the shear creep and attenuation behavior of polycrystalline olivine. Geophys Res Lett 27(15):2341–2344
Han DH, Liu J, Batzle M (2007) Shear velocity as the function of frequency in heavy oils, Soc. Exploration Geophys. Expanded Abstracts 26(1) doi:http://dx.doi.org/10.1190/1.2792824
Hessinger J, White BE Jr, Pohl RO (1996) Elastic properties of amorphous and crystalline ice films. Planet Space Sci 44:937–944. doi:10.1016/0032-0633(95)00112-3
Hiki Y, Tamura J (1983) Internal friction in ice crystals. J Phys Chem 87:4054–4059. doi:10.1021/j100244a011
Hurford TA, Helfenstein P, Hoppa GV, Greenberg R, Bills BG (2007) Eruptions arising from tidally controlled periodic openings of rifts on Enceladus. Nature 447:292–294. doi:10.1038/nature05821
Hussmann H, Spohn T (2004) Thermal-orbital evolution of Io and Europa. Icarus 171:391–410. doi:10.1016/j.icarus.2004.05.020
Jackson I (1993) Progress in the experimental study of seismic wave attenuation. Annu Rev Earth Planet Sci 21:375–406

Jackson I (2007) Physical origins of anelasticity and attenuation in rock. In: Schubert G (ed) Treatise of geophysics, vol 2, Mineral physics: properties of rocks and minerals. Elsevier, Amsterdam, pp 496–522, Chapter 2.17

Jackson I, Fitz Gerald JD, Faul UH, Tan BH (2002) Grain-size-sensitive wave attenuation in polycrystalline olivine. J Geophys Res 107(B12):2360. doi:1029/2001JB001225

Jackson I, Faul UH, Fitz Gerald JD, Tan BH (2004) Shear wave attenuation and dispersion in melt-bearing olivine polycrystals: specimen fabrication and mechanical testing. J Geophys Res 109: B06201

Jackson I, Faul UH, Fitz Gerald JD, Morris SJS (2006) Contrasting viscoelastic behavior of melt-free and melt-bearing olivine: implications for the nature of grain-boundary sliding. Mat Sci Eng A 442:170–174

James MR, Bagdassarov N, Müller K, Pinkerton H (2004) Viscoelastic behaviour of basalt lavas. J Volcanol Geotherm Res 132:99–113

Jellinek HHG, Brill R (1956) Viscoelastic properties of ice. J Appl Phys 27:1198–1209

Johari GP, Pascheto W, Jones SJ (1995) Anelasticity and grain boundary relaxation of ice at high temperatures. J Phys D-Appl Phys 28:112–119

Karato S (1998) A dislocation model of seismic wave attenuation and micro-creep in the Earth: Harold Jeffreys and the rheology of the solid earth. Pure Appl Geophys 153:239–256

Karato S (2008) Deformation of earth materials. Cambridge University Press, Cambridge, UK

Karato S, Spetzler HA (1990) Defect microdynamics in minerals and solid-state mechanisms of seismic wave attenuation and velocity dispersion in the mantle. Rev Geophys 28(4):399–421

Kê TS (1946) Experimental evidence of the viscous behavior of grain boundaries in metals. Phys Rev 71(8):533–546

Kê TS (1947) Experimental evidence of the viscous behavior of grain boundaries in metals. Phys Rev 71(8):533–546

Kê TS (1999) Fifty-year study of grain boundary relaxation. Metall Mater Trans A 30A:2267–2295

Knopoff L (1964) Q. Rev Geophys 4:625–660

Kuroiwa, D (1964) Internal friction of ice. I; The internal friction of H2O and D20 ice, and the influence of chemical impurities on mechanical damping. Contributions from the Institute of Low Temperature Science A18:1–37

Kuster GT, Toksöz MN (1974) Velocity and attenuation of seismic waves in two-phase media Part 1. Theoretical formulations. Geophysics 39:587

Ladanyi B, Saint-Pierre R (1978) Evaluation of creep properties of sea ice by means of a borehole dilatometer. In: Proceedings of the international association of hydraulic research symposium on ice problems, Part I, Lulea, pp 97–115

Lakes RS (1999) Viscoelastic solids. CRC Press, Boca Raton

Lakes RS (2004) Viscoelastic measurement techniques. Rev Sci Instrum 75(4):797–809

Langleben MP, Pounder ER (1963) Elastic parameters of sea ice, in ice and snow: properties, processes and applications. MIT Press, Cambridge, pp 69–78

Lee LC, Morris SJS (2010) Anelasticity and grain boundary sliding. Proc R Soc A. doi: rspa.2009.0624v1

Louchet F (2004) Dislocations and plasticity in ice. CR Phys 5:687–698

Mader HM (1992) Observations of the water-vein system in polycrystalline ice. J Glaciol 38 (130):333–347

Margot JL, Nolan MC, Benner LAM, Ostro SJ, Jurgens RF, Giorgini JD, Slade MA, Campbell DB (2002) Binary asteroids in the near-earth object population. Sci Exp. doi:10.1126/science.1072094

Matson DL, Castillo-Rogez JC, McKinnon WB, Sotin C, Schubert G (2009) The thermal evolution and internal structure of Saturn's midsize icy satellites. In: Brown R, Dougherty M, Esposito L, Krimigis T, Waite H (eds) Saturn after Cassini-Huygens, Springer, Chapter 19, doi:10.1007/978-1-4020-9217-6_18

Mavko GM (1980) Velocity and attenuation in partially melted rocks. J Geophys Res 85:5173–5189
Mavko G, Mukerji T, Dvorkin J (1998) The rock physics handbook: tools for seismic analysis of porous media. Cambridge University Press, Cambridge
Maxwell JC (1867) On the dynamical theory of gases. Philos Trans 157:49–83
McCarthy C, Goldsby DL, Cooper RF, Durham WB, Kirby SH (2007) Steady-state creep response of ice-I/magnesium sulfate hydrate. Workshop on ices, oceans, and fire: satellites of the outer Solar system, Boulder, 13–15 Aug 2007, pp 88–89
McCarthy C, Berglund SR, Cooper RF, Goldsby DL (2008) Influence of strain history and strain amplitude on the internal friction of ice-I and two-phase ice/salt hydrate aggregates, AGU fall meeting, American Geophysical Union
McCarthy C, Cooper RF, Goldsby DL, Durham WB, Kirby S (2011a) Transient and steady-state creep responses of ice-I and magnesium sulfate hydrate eutectic aggregates. J Geophys Res. doi:10.1029/2010JE003689
McCarthy C, Takei Y, Hiraga T (2011b) Experimental study of attenuation and dispersion over a broad frequency range: 2. The universal scaling of polycrystalline materials. J Geophys Res 116:1–18
McMillan KM, Lakes RS, Cooper RF, Lee T (2003) The viscoelastic behavior of β-In_3Sn and the nature of the high-temperature background. J Mater Sci 38:2747–2754
Meyer J, Wisdom J (2007) Tidal heating in Enceladus. Icarus 188:535–539
Meyer J, Wisdom J (2008) Episodic volcanism on Enceladus: Application of the Ojakangas-Stevenson model. Icarus 198:178–180
Mindlin RD (1954) Mechanics of granular media, Office of naval research project NR-064-388, Technical report no. 14, CU.-IA-i-i-ONR-266(09) –CE
Minster JB, Anderson DL (1981) A model of dislocation-controlled rheology for the mantle. Philos Trans Roy Soc Lond 299(1449):319–356
Montagnat M, Duval P (2004) Dislocations in ice and deformation mechanisms: from single crystals to polar ice. Defects Diffus Forum 229:43–54
Murray CD, Dermott SF (2000) Solar system dynamics. Cambridge University Press, Cambridge, UK, p 592
Nakamura T, Abe O (1980) A grain-boundary relaxation peak of antarctic mizuho ice observed in internal friction measurements at low frequency. J Fac Sci, Hokkaido University. Series 7, Geophysics 6(1):165–171
Niblett DH, Zein M (1980) The Bordoni peak in copper single crystals at megahertz frequencies. J Phys F Met Phys 10:773–780
Nimmo F (2008) Tidal dissipation and faulting, or a tale of Q and f. The science of Solar system ices workshop, Oxnard, 5–8 May 2008
Nimmo F, Spencer JR, Pappalardo RT, Mullen ME (2007) Shear heating as the origin of the plumes and heat flux on Enceladus. Nature 447:289–291
Nowick AS, Berry BS (1972) Anelastic relaxation in crystalline solids. Academic, New York
Nye JF, Frank FC (1973) Hydrology of the intergranular veins in a temperate glacier In: Symposium on the hydrology of glaciers, vol 95. Cambridge (1969), International Association of Scientific Hydrology Publication, pp 157–161
O'Connell RJ, Budiansky B (1977) Viscoelastic properties of fluid-saturated craced solids. J Geophys Res 82:5719–5735
O'Connell RJ, Budiansky B (1978) Measures of dissipation in viscoelastic media. Geophys Res Lett 5(1):5–8
Oguro M (2001) Anelastic behavior of H_2O ice single crystals doped with KOH. J Phys Chem Solids 62:897–902. doi:10.1016/S0022-3697(00)00247-X
Parameswaran VR (1987) Orientation dependence of elastic constants for ice. Def Sci J 37:367–375
Pauling L (1935) The structure and entropy of ice and other crystals with some randomness of atomic structure. J Am Chem Soc 57:2680–2684

Peale SJ (1986) Orbital resonances, unusual configurations and exotic rotation states among planetary satellites. In: Burns JA, Matthews MS (eds) Satellites. University of Arizona Press, Tucson

Peale SJ, Cassen P, Reynolds RT (1979) Melting of Io by tidal dissipation. Science 203:892–894

Peale SJ, Cassen P, Reynolds RT (1980) Tidal dissipation, orbital evolution, and the nature of Saturn's inner satellites. Icarus 43:65–72

Perez J, Maï C, Tatibouët J, Vassoille R (1986) Dynamic behaviour of dislocations in HF-doped ice Ih. J Glaciol 25(91):133–149

Petrenko VF, Whitworth RW (1999) Physics of ice. Oxford University Press, Oxford, UK

Pilbeam CC, Vaisnys JR (1973) Acoustic velocities and energy losses in gransular aggregates. J Geophys Res 78(5):810–824

Raj R (1975) Transient behavior of diffusion-induced creep and creep rupture. Metall Trans 6A:1499–1509

Raj R, Ashby MF (1971) On grain boundary sliding and diffusion creep. Metall Trans 2:1113–1127

Rambaux N, Castillo-Rogez JC, Williams JG, Karatekin O (2010) The librational response of Enceladus. Geophys Res Lett 37:L04202. doi:10.1029/2009GL041465

Rappaport NJ, Iess L, Wahr J, Lunine JI, Armstrong JW, Asmar SW, Tortora P, di Benedetto M, Racioppa P (2008) Can Cassini detect a subsurface ocean in Titan from gravity measurements? Icarus 194:711–720. doi:10.1016/j.icarus.2007.11.024

Roberts JH, Nimmo F (2008) Tidal heating and the long-term stability of a subsurface ocean on Enceladus. Icarus 193:675–689

Robuchon G, Choblet G, Tobie G, Cadek O, Sotin C, Grasset O (2010) Coupling of thermal evolution and despinning of early Iapetus. Icarus 207:959–971. doi:10.1016/j.icarus.2009.12.002

Romanowicz B (1994) Anelastic tomography: a new perspective on upper-mantle thermal structure. Earth Planet Sci Lett 128:113–121

Rothrock DA (1975) Mechanical behavior of pack ice (invited review paper). Annu Rev Earth Planet Sci 3:317–342

Schulson EM, Duval P (2009) Creep and fracture of ice. Cambridge University Press, Cambridge, UK

Snoek J (1939) Letter to the editor. Physica 6(7–12):591–592. doi:10.1016/S0031-8914(39)90061-3

Song M (2008) An evaluation of the rate-controlling flow process in Newtonian creep of polycrystalline ice. Mater Sci Eng A Struct Mater Propert Microstr Process 486:27–31

Song M, Cole DM, Baker I (2006) Investigation of Newtonian creep in polycrystalline ice. Philos Mag Lett 86:763–771

Sotin C, Head JW, Tobie G (2002) Europa: tidal heating of upwelling thermal plumes and the origin of lenticulae and chaos melting. Geophys Res Lett 29:74-1. doi:10.1029/2001GL013844, CiteID 1233

Spencer JR, Pearl JC, Segura M, Flasar FM, Mamoutkine A, Romani P, Buratti BJ, Hendrix AR, Spilker LJ, Lopes RMC (2006) Cassini encounters enceladus: background and the discovery of a South Polar hot spot. Science 311:1401–1405

Spetzler H, Anderson DL (1968) The effect of temperature and partial melting on velocity and attenuation in a simple binary system. J Geophys Res 73:6051–6060

Staroszczyk R, Morland L (1999) Orthotropic viscous model for ice, Lecture notes in physics, technological, environmental, and climatological impact. In: Proceedings of the 6th international symposium, Darmstadt, 22–25 Aug 1999, pp 249–258, doi:10.1007/BFb0104166

Sundberg M, Cooper RF (2010) A composite viscoelastic model for incorporating grain boundary sliding and transient diffusion creep; correlating creep and attenuation responses for materials with a fine grain size. Philos Mag 90(20):2817–2840

Tamura J, Kogure Y, Hiki Y (1986) Ultrasonic attenuation and dislocation damping in crystals of ice. J Phys Soc Jpn 55(10):3445–3461

Tan BH, Jackson I, Fitz Gerald JD (2001) High-temperature viscoelasticity of fine-grained polycrystalline olivine. Phys Chem Miner 28:641–664

Tatibouet J, Perez J, Vassoille R (1981) Very low frequencies internal friction measurements of ice Ih. J Phys Colloq C5(42):541–546
Tatibouet J, Perez J, Vassoille R (1983) Study of lattice defects in ice Ih by very-low-frequency internal friction measurements. J Phys Chem 87:4050–4054
Tatibouet J, Perez J, Vassoille R (1986) High-temperature internal friction and dislocations in ice Ih. J Phys 47:51–60
Tatibouet J, Perez J, Vassoille R (1987) Study of grain boundaries in ice by internal friction measurement. J Phys 48(suppl 3):C1-197–C1-203
Taupin V, Richeton T, Chevy J, Fressengeas C, Weiss J, Louchet F, Carmen-Miguel M (2008) Rearrangement of dislocation structures in the aging of ice single crystals. Acta Mater 56:1555–1563
Tobie G, Choblet G, Sotin C (2003) Tidally heated convection: constraints on Europa's ice shell thickness. J Geophys Res 108:5124. doi:10.1029/2003JE002099
Tobie G, Mocquet A, Sotin C (2005) Tidal dissipation within large icy satellites: applications to Europa and Titan. Icarus 177:534–549
Tobie G, Cadek O, Sotin C (2008) Solid tidal friction above a liquid water reservoir as the origin of the south pole hotspot on Enceladus. Icarus 196:642–652
Vassoille R, Mai C, Perez J (1978) Inelastic behavior of ice Ih single crystals in the low-frequency range due to dislocations. J Glaciol 21(85):375–384
Waff HS, Bulau JR (1979) Equilibrium fluid distribution in an ultramafic partial melt under hydrostatic stress conditions. J Geophys Res 84:6109–6114
Webb WW, Hayes CE (1967) Dislocations and plastic deformation of ice. Philos Mag 16:909–925
Webb S, Jackson I (2003) Anelasticity and microcreep in polycrystalline MgO at high temperature: an exploratory study. Phys Chem Miner 30:157–166. doi:10.1007/s00269-003-0299-1
Weertman J (1955) Internal friction of metal single crystals. J Appl Phys 26(2):202–210
Weertman J (1983) Creep deformation of ice. Annu Rev Earth Planet Sci 11:215–240
Weertman J, Weertman JR (1975) High temperature creep of rock and mantle viscosity. Annu Rev Earth Planet Sci 3:293–315
Whitworth RW (1980) The influence of the choice of glide plane on the theory of the velocity of dislocations in ice. Philos Mag A 41(4):521–528
Wieczerkowski K, Wolf D (1998) Modelling of stresses in the Fennoscandian lithosphere induced by Pleistocene glaciations. Tectonophysics 294(3–4):291–303
Williams JG, Boggs DH, Yoder CF, Ratcliff JT, Dickey JO (2001) Lunar rotational dissipation in solid body and molten core. J Geophys Res-Planet 106:27933–27968
Winkler KW, Murphy WF III (1995) Acoustic velocity and attenuation in porous rocks. In: Ahrens TJ (ed) Rock physics and phase relations: A handbook of physical constants. American Geophysical Union, Washington, DC
Woirgard J, Sarrazin Y, Chaumet H (1977) Apparatus for the measurement of internal friction as a function of frequency between 10^{-5} and 10 Hz. Rev Sci Instrum 48(10):1322–1325
Wu TT (1966) The effect of inclusion shape on the elastic moduli of a two-phase material. Int J Solids Struct 2:1–8
Yoder CF (1982) Tidal rigidity of Phobos. Icarus 49:327–346
Zener C (1947) Theory of the elasticity of polycrystals with viscous grain boundaries. Phys Rev 60:906–908
Zener C (1948) Elasticity and anelasticity of metals. University of Chicago Press, Chicago
Zhang K, Nimmo F (2009) Recent orbital evolution and the internal structures of Enceladus and Dione. Icarus 204:597–609. doi:10.1016/j.icarus.2009.07.007
Zschau J (1978) Tidal friction in the solid earth: loading tides versus body tides. In: Brosche P, Sundermann J (eds) Tidal friction and the Earth's rotation. Springer, New-York, pp 62–94